Kinematics of the Aspen Grove Landslide, Ephraim Canyon, Central Utah

U.S. GEOLOGICAL SURVEY BULLETIN 1842–F

Chapter F

Kinematics of the Aspen Grove Landslide, Ephraim Canyon, Central Utah

By REX L. BAUM, ROBERT W. FLEMING, and ARVID M. JOHNSON

Description and analysis of deformational structures and of spatial and temporal patterns of movement of the landslide

U.S. GEOLOGICAL SURVEY BULLETIN 1842

LANDSLIDE PROCESSES IN UTAH—OBSERVATION AND THEORY

U.S. DEPARTMENT OF THE INTERIOR
BRUCE BABBITT, Secretary

U.S. GEOLOGICAL SURVEY
Robert M. Hirsch, Acting Director

UNITED STATES GOVERNMENT PRINTING OFFICE: 1993

For sale by
USGS Map Distribution
Box 25286, Building 810
Denver Federal Center
Denver, CO 80225

Library of Congress Cataloging-in-Publication Data

Baum, Rex L.
Kinematics of the Aspen Grove landslide, Ephraim Canyon, central Utah : description and analysis of deformational structures and of spatial and temporal patterns of movement of the landslide / by Rex L. Baum, Robert W. Fleming, and Arvid M. Johnson.
p. cm. — (U.S. Geological Survey bulletin ; 1842)
Includes bibliographical references.
Supt. of Docs. no.: I19.3:1842-F
1. Landslides—Utah—Ephraim Canyon. I. Fleming, Robert W. II. Johnson, Arvid M. III. Title. IV. Series.
QE75.B9 no. 1842
[QE599.U5]
557.3 s—dc20
[551.3'07]

93-24966
CIP

CONTENTS

Abstract **F1**
Introduction **F1**
Acknowledgments **F4**
Timing of landslide activity **F4**
Generally steady movement in main body of landslide **F7**
Pattern of displacement **F9**
Distributed shear within the landslide debris **F12**
Localized deformation **F17**
    Deformation in ground being extended **F17**
    Deformation in ground being shortened **F21**
    Deformation at a flank ridge **F21**
    Deformation over a bump in the failure surface **F23**
Discussion and conclusion **F25**
References cited **F29**
Appendix **F34**

PLATE

[Plate is in pocket]

F1. Map showing approximate boundaries and displacement of points at the surface of the Aspen Grove landslide from 1983 through 1986

FIGURES

F1. Plane-table map showing structural features of the Aspen Grove landslide, August 1984 **F2**
F2. Map showing location of the Aspen Grove landslide **F4**
F3. Graph showing the timing of measurements in relation to the activity of the landslide **F6**
F4. Graph of displacement at extensometer E1, showing the seasonal beginning of sliding on March 26, 1986 **F7**
F5. Graph of displacement at extensometer E6 during 1986 **F7**
F6. Plane-table map showing locations of extensometers E1, E2, and E3 **F8**
F7–F13. Graphs:
    F7. Displacements measured by extensometers E1, E2, and E3 during late April and early May 1985 **F9**
    F8. Average daily velocities at extensometers E1, E2, and E3 during 1985 **F10**
    F9. Average daily velocities at quadrilaterals Q–2 and Q–6 during part of 1983 **F11**
    F10. Average daily velocities at quadrilaterals Q–2, Q–6, and Q–29, and at the split tree on the left flank, during part of 1984 **F11**
    F11. Displacements at extensometers E2 and E3 on the evening of July 13, 1985 **F12**
    F12. Normalized annual displacement of points at the surface of the Aspen Grove landslide from 1983 to 1986 **F13**
    F13. Displacement of transverse lines of stakes in the upper, middle, and lower parts of the Aspen Grove landslide **F14**

F14. Sketch and graph showing parameters used in analysis of flow in converging and diverging channels **F15**
F15. Graphs comparing observed deformation at transverse lines of stakes to theoretical plastic deformation in converging or diverging channels **F16**
F16–F19. Plane-table maps of the Aspen Grove landslide:
F16. Development of scarps in ground stretching longitudinally near station 170 **F18**
F17. Head of the landslide, August 1984 **F20**
F18. Topography and structures in ground near line M (station 390) that was shortening longitudinally **F21**
F19. Flank ridge near station 150 in August 1984 **F22**
F20. Profiles and vertical displacement graphs of lines R1, R2, and R3 **F24**
F21. Graph showing difference in height between stakes 1 and 2 of line R2 compared to downslope displacement **F25**
F22. Plane-table maps of the flank ridge near station 150 in August 1985 **F26**
F23. Graph showing lateral strain in stake lines R1, R2, and R3 on the flank ridge **F27**
F24. Schematic diagram showing helical flow pattern indicated by displacement of points on the surface of the flank ridge **F27**
F25. Graph comparing deformation at the ground surface above a theoretical intrusion with deformation at line R1 on the ridge **F28**
F26. Plane-table map of the dome near station 250 at the beginning of movement in 1985 **F29**
F27. Photograph, looking north, of leaning trees on the dome in July 1985 **F30**
F28. Profiles of stake lines across the dome near station 250 showing displacement between April and August 1985 **F31**
F29. Diagram showing how trees that were initially vertical are tilted as the landslide moves over a bump on the slip surface **F31**
F30. Plane-table maps of the dome near station 250 as of August 2, 1985 **F32**

TABLES

F1. Instrumentation used to measure velocity, displacement, and strain in the Aspen Grove landslide **F5**
F2. Seasonal beginning and end of movement of the Aspen Grove landslide from 1983 through 1986 **F6**
F3. Displacement of stakes in quadrilateral Q–2 on the flank ridge near station 120 **F28**

CONVERSION FACTORS

For the convenience of readers, the metric units used in this report may be converted to inch-pound units by using the following factors:

Multiply metric units	By	To obtain inch-pound units
mm (millimeters)	0.03937	inches
cm (centimeters)	0.3937	inches
m (meters)	3.2808	feet
km (kilometers)	0.6214	miles
cm/s^2 (centimeters per second per second)	0.03281	feet per second per second
cm/d (centimeters per day)	0.3937	inches per day
cm/d^2 (centimeters per day per day)	0.3937	inches per day per day
m/h (meters per hour)	9.113×10^{-4}	feet per second
radians	57.296	degrees (°)

Kinematics of the Aspen Grove Landslide, Ephraim Canyon, Central Utah

By Rex L. Baum,[1] Robert W. Fleming,[1] *and* Arvid M. Johnson[2]

Abstract

The Aspen Grove landslide in central Utah is a long, narrow landslide that moved during the spring and summer months of 1983–86. Each year, the landslide started moving at about the time that the snow melted, accelerated to a peak velocity of about 20 centimeters per day during May or early June, and slowed gradually until it stopped moving in July or August. The landslide was practically in mechanical equilibrium throughout its period of activity; movement was relatively steady rather than surging.

Much of the deformation of the landslide is controlled by the geometry of the landslide boundaries, which persisted from year to year. Movement was primarily by boundary shear (sliding) rather than flow; from 82 to 97 percent of the displacement at the axis is due to shear at the boundaries of the landslide. Many deformational features at the surface of the landslide can be understood in terms of simple kinematic models that account for the sliding motion and irregular boundaries of the landslide. Points on the surface of the landslide were displaced each year in approximately the same spatial pattern, but the amount of displacement varied from year to year. The spatial pattern of displacement was determined largely by variation in the width and thickness of the landslide; however, localized events, such as rapid development of the head during 1984, caused the spatial pattern to vary slightly from year to year. Transverse velocity profiles in sections of the landslide that have converging or diverging boundaries are consistent with models for plastic deformation in a converging or diverging channel. Several bumps and depressions on the surface of the landslide mimicked bumps and depressions in the basal slip surface.

Longitudinal stretching and shortening are common styles of deformation in many landslides, and recognition of these styles aids in estimating the horizontal stresses in an active landslide. The upslope half of the landslide stretched longitudinally and the downslope half shortened. Plane-table maps document the evolution of grabens, cracks, and normal faults that formed in ground being stretched. Where the landslide was shortening, it became thicker, and shallow thrust faults and buckles appeared at the surface.

Ridges formed locally along the flanks of the landslide. Flank ridges are common landslide features, and though they are still poorly understood, our observations show how the ridges can form. One of these ridges grew approximately 12 cm in height as a result of 7 m of displacement from 1984 to 1986. Details of the deformation rule out buckling and helical flow as mechanisms for forming this ridge, but are consistent with a model for intrusion of material beneath the ridge.

INTRODUCTION

Displacements, strains, and velocities of a landslide determine the way the landslide moves and deforms, in short, the kinematics of the landslide. Here we describe the kinematics of the Aspen Grove landslide in Ephraim Canyon, Utah (figs. F1 and F2). We have described the dimensions, features, and setting of the Aspen Grove landslide in other chapters of this bulletin (Baum and others, 1988; Baum and Fleming, 1989).

We began our study of the Aspen Grove landslide to assess its potential as a hazard, rather than to understand its kinematics. In June 1983, the landslide was one of several landslides in Ephraim Canyon that damaged roads and disrupted the water supply of the city of Ephraim. At that time, the landslide was enlarging; we were interested in how large the landslide might become and how fast and far it might move. It turns out that the landslide never moved very fast or far during any period of activity. Thus, we were able to observe surficial features such as cracks and bulges that were created and destroyed by movement of the landslide.

Our study of kinematics evolved as we observed interesting aspects of the landslide. Initially, we monitored the movement with a few wooden stakes set out as quadrilaterals and by plane-table mapping. Later, we

[1]U.S. Geological Survey, Box 25046, MS 966, Denver, CO 80225.
[2]Purdue University, Department of Earth and Atmospheric Sciences, CIVL Building, West Lafayette, IN 47907.

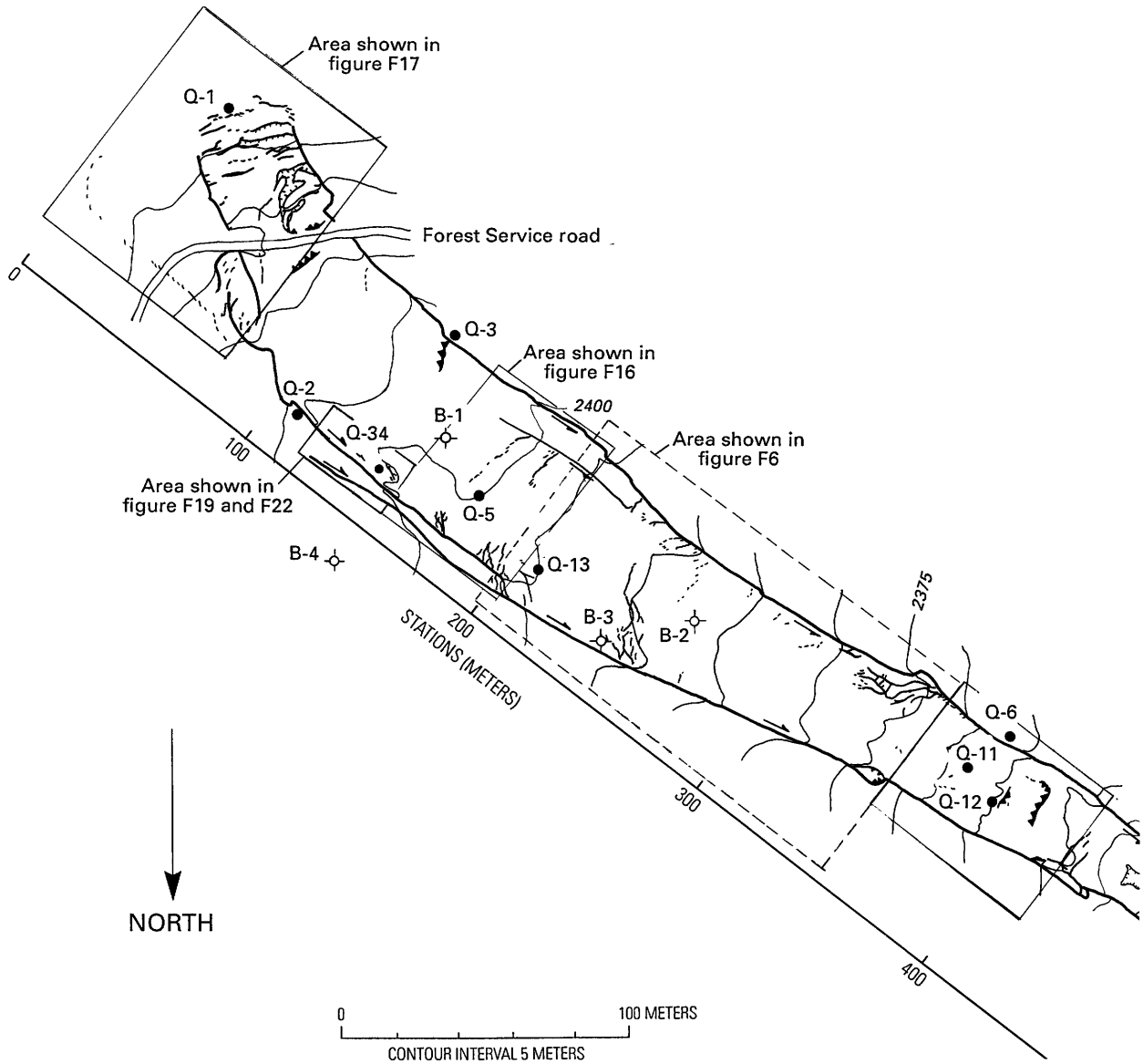

Figure F1 (above and facing page). Plane-table map showing structural features of the Aspen Grove landslide near Ephraim, Utah, August 1984. Movement of the landslide is toward the northwest (from the upper-left to the lower-right corner of the map). Note that left and right halves of map overlap. See figure F2 for location.

added more instrumentation as our questions and observations became more pointed and specific. By the time the Aspen Grove landslide had finished its 1986 movement episode, we had accumulated data on the following topics relevant to its kinematics:

1. The timing of movement in different parts of the landslide.
2. The rate and steadiness of movement.
3. The spatial distribution of displacement.
4. The gross pattern of longitudinal strain and the homogeneity of strain.
5. Internal shearing of the landslide debris.
6. The evolution of deformational features in ground being stretched and in ground being shortened.
7. The formation of flank ridges.
8. Deformation at the ground surface caused by bumps and depressions on the slip surface of the landslide.
9. Enlargement of the landslide.

Our data on these topics are useful for several different purposes. In combination, data on the timing of movement, the spatial pattern of movement, and the enlargement of the landslide help determine which parts of the landslide were driving the movement. Data on the rate and steadiness of movement determine whether the

landslide was in mechanical equilibrium while it was active, as well as determining whether surging or stick-slip play significant roles in the movement (Keefer and Johnson, 1983, p. 47). The amount of internal shearing of the landslide determines the relative importance of sliding and flowing as mechanisms of movement. Data on the evolution of deformational features in zones of longitudinal stretching and shortening, the formation of flank ridges, and deformation of the ground surface caused by topographic features of the slip surface document the evolution of features common to many landslides we have observed in Utah and elsewhere. Recognition of zones of longitudinal stretching and shortening aids in the determination of appropriate values of interslice forces in stability analysis of landslides (Baum and Fleming, 1991). Identification of bumps and depressions on the slip surface aids in determining the shape of the slip surface of a landslide.

We used three kinds of instruments in this study to determine displacements, strains, and velocities at the surface of the Aspen Grove landslide: quadrilaterals of stakes indicated displacement along the boundaries of the slide or strain at points on the surface of the landslide (Johnson

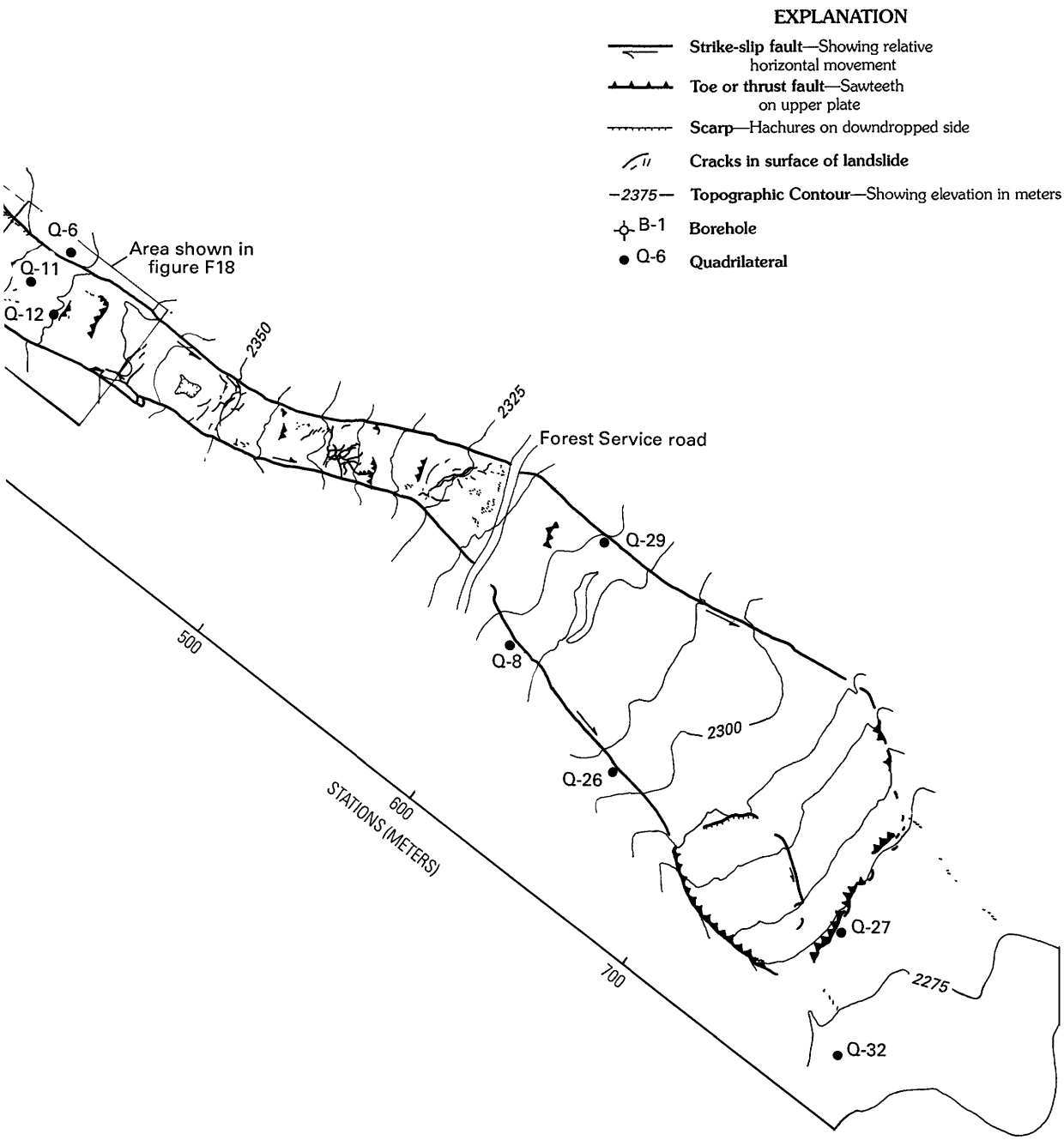

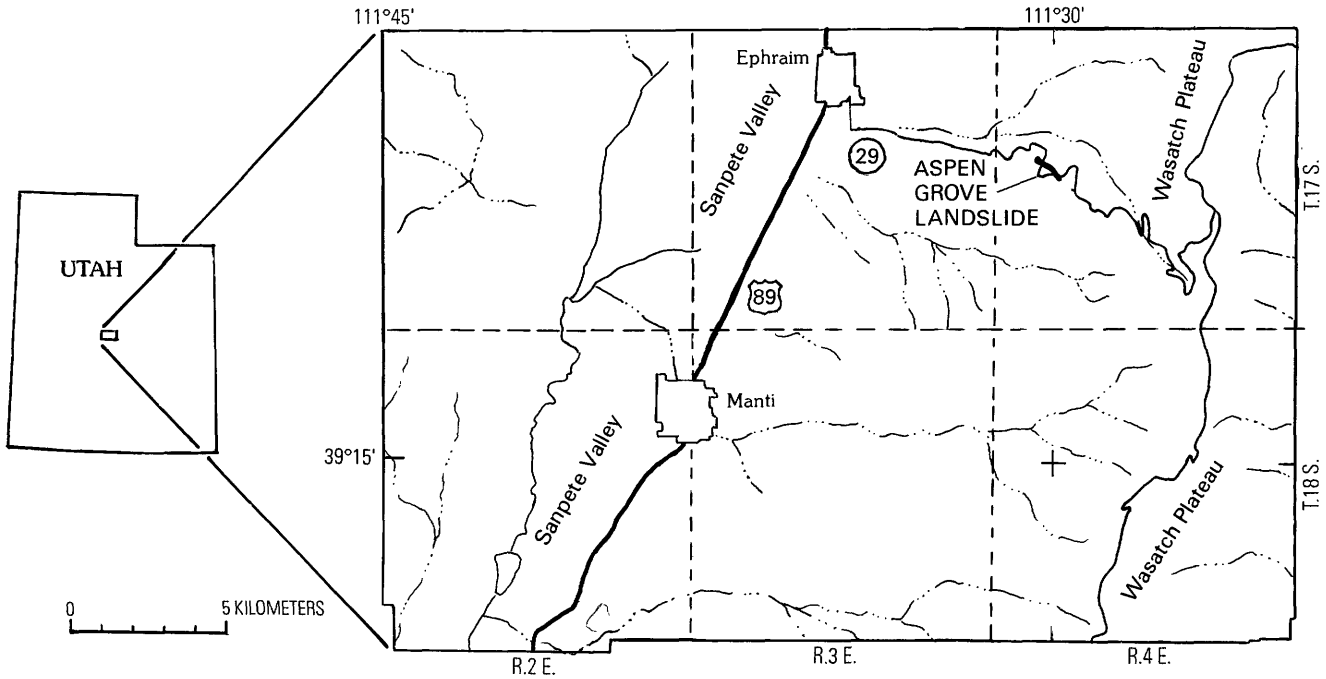

Figure F2. Location of the Aspen Grove landslide, on the west side of the Wasatch Plateau, central Utah.

and Baum, 1987; Baum and others, 1988); stake lines indicated displacement as well as one-dimensional strain; and recording extensometers indicated velocity (see appendix). We used instruments in various combinations to make measurements needed to answer each of our questions. In many cases we supplemented the instrumental measurements with photographs and plane-table maps of the surface of the landslide to document changes in deformational features. A byproduct of repeated plane-table mapping was that stakes and other identifiable points shown on the maps served as supplemental indicators of annual displacement. Locations of quadrilaterals, stake lines, and extensometers used are shown on plate F1; the period of use and specific purpose of each are listed in table F1. The accuracy of various kinds of measurements is discussed in the appendix. Station numbers indicate the distance, in meters, from the crown of the landslide (table F1, plate F1). Right and left refer to an observer facing downslope (Varnes, 1978).

The landslide was monitored for several months each year for five years (1983–87). In general, we tried to begin measurement before movement started in the spring and to continue monitoring as long as movement continued. Unfortunately, movement began while the stakes were still buried by the winter snowpack, but we were able to document the beginning of movement one year with recording extensometers. By comparing measurements from the end of monitoring one season to the beginning of monitoring the next season, we were able to determine the amount of movement during the nonmonitored periods (mainly autumn and winter). The times of different types of measurements and landslide activity for the period 1983–86 are shown in figure F3. During 1987, the landslide did not move.

ACKNOWLEDGMENTS

We were assisted in the field by David J. Varnes, Roger Nichols, and Lee-Ann Bradley of the U.S. Geological Survey, Denver, Colo.; Roger Johnson and Chad Perry of Ephraim, Utah; and Douglas Robins of Gunnison, Utah. Roger Nichols also managed the field instrumentation. Manti District Ranger Ben Black and Gary Jorgenson, both with the U.S. Forest Service in Ephraim, Utah, shared observations and helped solve various logistical problems. We express our sincere appreciation to all these people.

TIMING OF LANDSLIDE ACTIVITY

Each year from 1983 through 1986, the Aspen Grove landslide moved for about 3 to 5 months, between about April and August (fig. F3). The beginning of movement coincided approximately with melting of the winter snowpack, which generally occurs during March, April, or May. Movement ended during the summer after the ground surface had become dry and hard. A few data are

Table F1. Instrumentation used to measure velocity, displacement, and strain in the Aspen Grove landslide

Instrument	Period of use	Station	Purpose
Quadrilaterals[1]			
Q–1	6/83–9/86	25	Displacement at head.
Q–2	6/83–9/86	115	Displacement on right flank.
Q–3	6/83–9/86	135	Displacement on left flank.
Q–4	6/83–9/86	120	Strain at line U.
Q–5	6/83–9/86	180	Strain at top of bump on surface of landslide.
Q–6	6/83–9/86	375	Displacement of left flank at line M.
Q–7	6/83–9/86	600	Displacement on left flank near projected location of toe.[2]
Q–8	6/83–8/85	595	Displacement on right flank near projected location of toe.
Q–9	6/83–9/86	580	Strain approximately 30 m upslope from projected location of toe.
Q–10	6/83–8/83, 4/85–9/86	380	Strain adjacent to left flank at line M.
Q–11	6/83–9/86	375	Strain at axis near line M.
Q–12	6/83–9/86	380	Strain at axis along line M.
Q–13	6/83–9/86	210	Strain.
Q–14	6/83–9/86	210	Strain.
Q–26	5/84–9/86	655	Displacement on right flank.
Q–27	5/84–9/86	755	Displacement on internal toe.
Q–28	5/84–9/86	690	Displacement on left flank.
Q–29	5/84–9/86	595	Displacement on left flank, replaced Q–7.[2]
Q–32	5/84–9/86	790	Displacement on right flank.
Q–33	6/84–9/86	150	Strain at a flank ridge.
Q–34	6/84–9/86	135	Do.
Q–35	6/84–8/85	160	Experiment with use of large quadrilateral to measure strain.
Q–85	4/85–9/86	155	Displacement on new right flank.
Q–86	4/85–9/86	245	Strain on side of dome.
Q–87	4/85–9/86	775	Displacement on left flank.
Stake lines[3]			
Line C..	6/83–9/86	10–45	Displacement of head, strains in crown.
Line U..	6/83–9/86	125	Compare internal shearing with displacement at boundaries.
Line M.	6/83–9/86	380	Do.
Line L..	6/83–9/86	600	Do.
Line LL	6/83–9/86	580–600	Observe shortening at predicted location of toe.
Line R1	6/84–9/86	150	Observe deformation of flank ridge.
Line R2	6/84–9/86	137	Do.
Line R3	4/85–9/86	155	Do.
Line DT	4/85–9/86	245	Observe deformation of dome.
Line DL	4/85–9/86	245	Do.
Extensometers[4]			
E1	4/85–8/85, 2/86–9/86	215	Timing and rate of movement.
E2	4/85–8/85, 2/86–9/86	285	Do.
E3	4/85–8/85, 2/86–9/86	325	Do.
E4	4/85–8/85	790	Do.
E5	4/85–8/85	830	Do.
E6	4/85–8/85, 2/86–9/86	880	Do.

[1]Measured every 2–3 days in 1983 and 1984, and approximately monthly in 1985 and 1986. Raw quadrilateral measurements are tabulated in appendix C of Baum (1988).

[2]During 1984, the left flank developed outside of Q–7, so Q–29 was installed to monitor displacement on the left flank and Q–7 was used to monitor strain near the left flank.

[3]Measured once every 2 or 3 days in 1983, and weekly, monthly, or annually thereafter.

[4]Recorded displacement every 15 min. Most were disabled for brief intervals during the period of use. Extensometers E4 and E5 yielded no useful data.

available to constrain the beginning and end of movement episodes.

Dates when movement started in 1983, 1984, and 1985 (table F2) are estimates because movement started before we could begin monitoring the landslide. We estimated the dates in table F2 by dividing the rate the slide was moving when we began to monitor it, into the displacement since movement had halted the previous year, to estimate the number of days the slide might have been moving before monitoring began. The slide was usually accelerating when we began monitoring, so movement probably started before the estimated dates.

The first movement in the main body of the landslide was well documented in 1986. Extensometer E1 (fig. F4) showed no changes from February 12 until about March 19, when minor fluctuations began. Undeniable downslope movement began on March 26 and continued until at least March 31, when the extensometer broke (fig. F4).

The distal part of the landslide started moving at least a day later (March 27) and probably 2 weeks later than the main body in 1986 (fig. F5). Although the extensometer there did not record the actual start of movement, because its clock was not working from March 27 to April 18, extrapolation of the steep part of the extensometer curve (fig. F5) indicates that movement started about April 10.

The end of movement was fairly well documented in 1983 and 1985 (table F2). Our data for 1983 and 1985 indicate that different parts of the landslide stopped at different times. In 1983, movement near station 120 (Q–2) stopped about a week before movement near station 390 (Q–6). In 1985, movement near the terminus (E6, pl. F1) stopped about a month before movement in the wedge segment (E2 and E3).

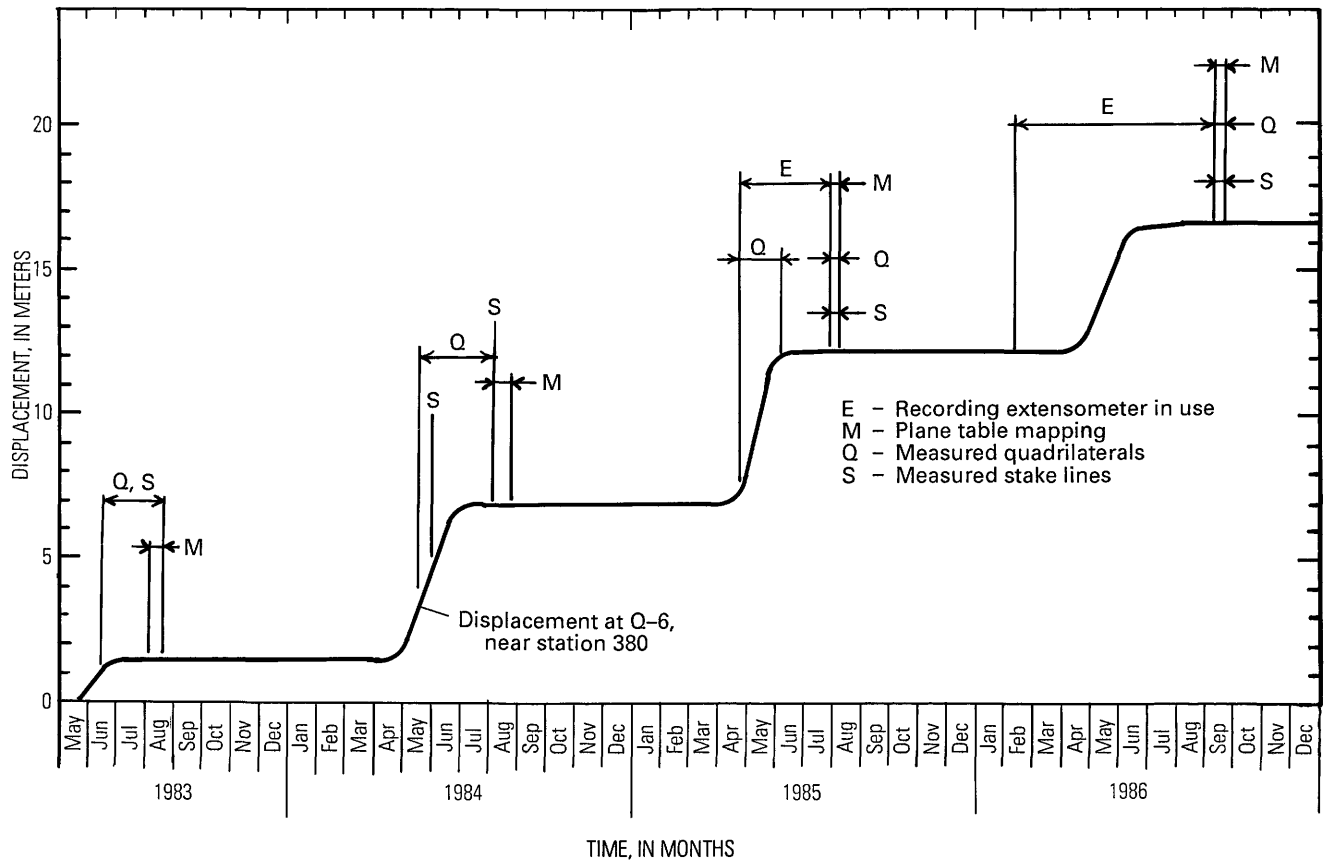

Figure F3. Timing of measurements in relation to the activity of the Aspen Grove landslide. The heavy curved line indicates the displacement at Q–6, near midlength of the landslide (fig. F1, pl. F1). Vertical lines indicate the beginning and ending times of plane-table mapping, measurement of stake lines and quadrilaterals, and operation of extensometers. The landslide generally was active from early spring to late summer, and measurements were performed during the spring and summer.

Table F2. Seasonal beginning and end of movement of the Aspen Grove landslide from 1983 through 1986

Year	First observed evidence of movement				Latest probable starting date[1]	Last observed evidence of movement	
	Location	Date	Displacement since start (cm)	Rate of movement (cm/d)		Location	Date
1983	Lower road crossing	May 31	[2]10-20	Unknown	May 31	Quadrilateral Q-2	July 15
						Quadrilateral Q-6	July 23
1984	Split tree	May 16	50	10	May 11	Stations 0-400[3]...	August 10
1985	Extensometer E3	April 23	[4]70	8	April 14	Extensometer E6	June 25
						Extensometer E3	July 29
						Extensometer E2	July 31
1986	Extensometer E1	March 26	0	0.2	March 26[5]	Extensometer E6	June 10-20
	Extensometer E6	April 18	5	0.6	April 10[6]		

[1]Assuming rate of movement was constant from start of movement to first observation.
[2]Estimated from observations of crack development as a function of increasing displacement.
[3]Evidence of movement comprised cracks in fresh mud along the flanks and the sounds of tree roots breaking in the head of the landslide.
[4]Estimated by subtracting displacement at E3 from April 23 to April 28 from displacement at Q-6 from August 1984 to April 28.
[5]See figure F4.
[6]See figure F5.

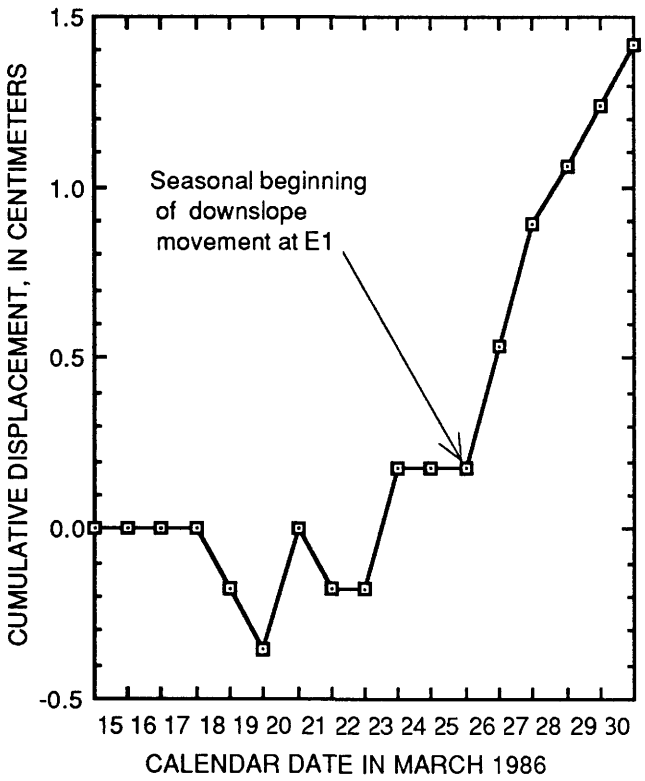

Figure F4. Displacement at extensometer E1, showing the seasonal beginning of sliding on March 26, 1986. The extensometer measured displacement in increments of 0.18 cm. Extensometer readings at 12:00 midnight, at the beginning of each day, indicate the daily displacement.

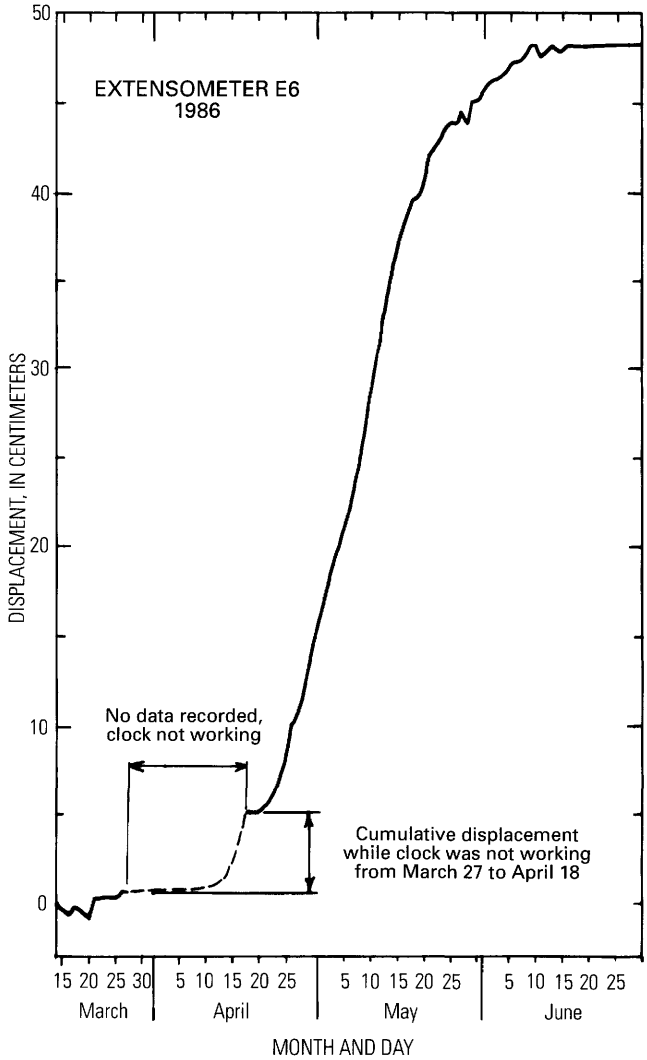

Figure F5. Displacement at extensometer E6 during 1986. The extensometer recorded displacement every 15 min in increments of approximately 0.3 cm. Peaks and troughs in the extensometer record during periods of relatively slow movement represent times when the extensometer wire was temporarily deflected and later returned to its normal, taut position. The clock that controlled data collection at extensometer E6 worked from February 12 until it broke on March 27. Movement began after March 27 but before clock was replaced on April 18. The extensometer continued to work while the clock was broken, so the 5 cm of movement that accumulated between March 27 and April 18 was registered when the clock was replaced. Movement probably began about April 10 and ended about June 11.

GENERALLY STEADY MOVEMENT IN MAIN BODY OF LANDSLIDE

We observed the rate of movement of the landslide to determine whether the landslide moves steadily (Keefer and Johnson, 1983, p. 47) or in surges (Hutchinson, 1970; Hutchinson and others, 1974; Prior and Stephens, 1972) and to determine whether the landslide was in mechanical equilibrium while it was active. During much of the spring of 1985, we observed the rate of movement in detail by using three extensometers (appendix). The extensometers were on the right flank in the wedge segment of the landslide (fig. F6).

The extensometer records show that sudden movements were uncommon and that the landslide usually accelerated and decelerated gradually (fig. F7). The displacement curves are relatively smooth, even during the period of most rapid movement. Smooth acceleration also was recorded in 1986 at extensometer E6, which was on the right flank near the toe of the landslide (fig. F5).

Average daily velocities were calculated for extensometers E1, E2, and E3, and these are shown on the graphs in figure F8. The landslide gradually accelerated to a peak velocity of 16.5–20 cm/d on May 4, and then gradually slowed during May, June, and July. Daily average accelerations were as great as 5 cm/d^2, but commonly

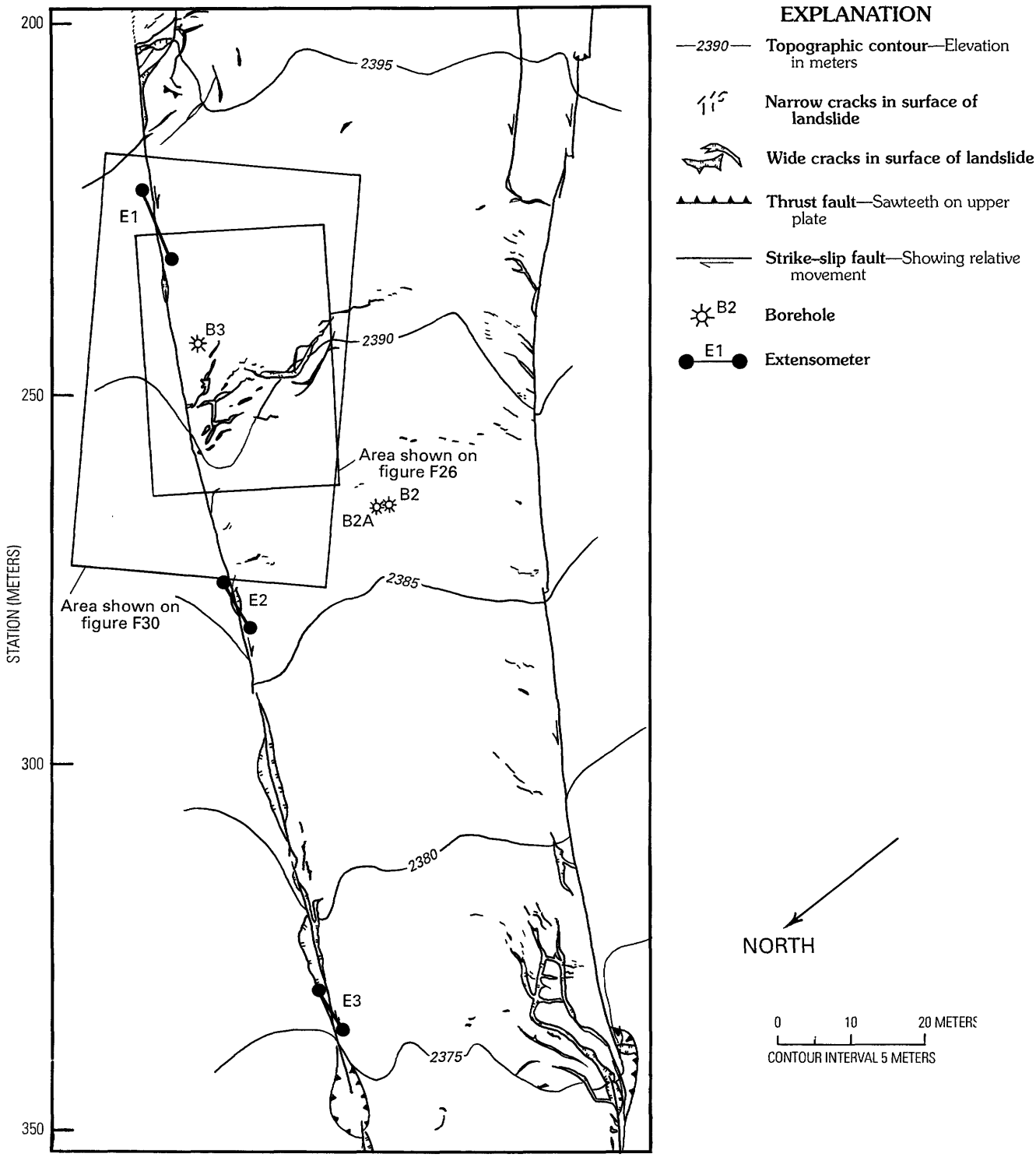

Figure F6. Plane-table map showing locations of extensometers E1, E2, and E3 and physical features of the landslide in their vicinity. The extensometers were on the right flank about 210–350 m downslope from the head. See figure F1 for location of map area.

were less than 1.5 cm/d^2. This same general pattern of gradual acceleration to a peak velocity followed by gradual slowing appears to have been followed each year (figs. F9 and F10). The peak velocity lasted only one day, and apparently there was no time of true steady-state movement. Indeed, the fact that movement started and stopped at different times in different parts of the landslide indicates that movement was unsteady.

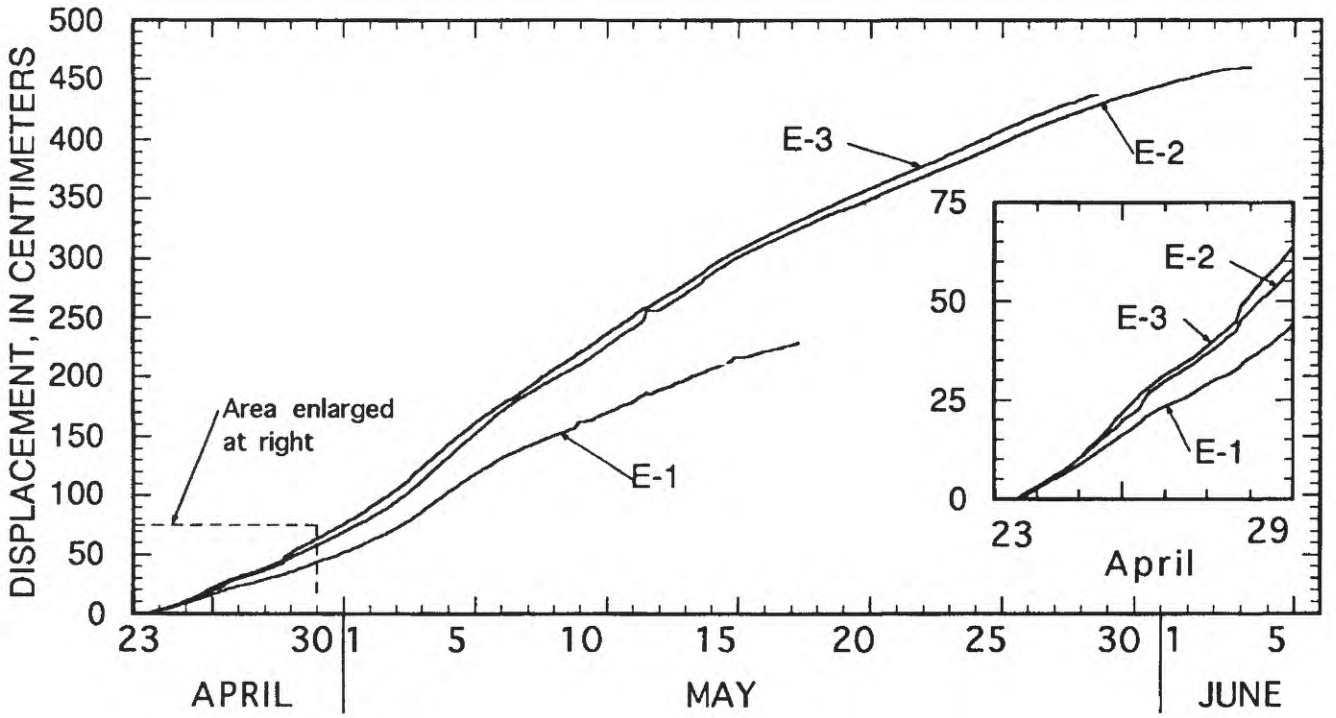

Figure F7. Displacements measured by extensometers E1, E2, and E3 during late April and early May 1985. Movement was relatively steady; most of the small bumps on the curve result from the incremental record of the extensometers. The extensometers register changes of displacement in increments of approximately 0.18 cm, and they record displacement at intervals of 15 min. A few of the larger bumps on the curves apparently resulted from rapid movements amounting to about 1–3 cm in 15–30 min.

A possible occurrence of sudden propagating movement was recorded by extensometers E2 and E3 (fig. F11) on the evening of July 13, 1985. Unfortunately, the event was not recorded at E1, which was disabled in July. The changes at E2 and E3 occurred in less than the time the extensometers can resolve (within 15 minutes); thus, the nature of the recorded changes is uncertain (fig. F11). However, if the two incidents do reflect wavelike propagation of a sudden movement, then a zone of rapid movement propagated down the slope from E2 to E3 at a speed of about 34–56 meters per hour. We have no other explanations for the phenomenon, and we know of no major storms or other external causes that would produce the changes measured.

The landslide was virtually in mechanical equilibrium throughout its period of movement. Acceleration of the landslide was small compared to gravity throughout the period of movement. The velocity fluctuated a small amount from hour to hour and day to day. Except for the possible abrupt movement described above, the greatest acceleration recorded by the extensometers occurred during late April 1985. The acceleration was 1.6×10^{-7} cm/s^2. This is negligible compared to the component of the acceleration due to gravity that is tangent to the slope (204 cm/s^2, assuming a slope of about 12°). Acceleration ranging from 9.9×10^{-6} to 8 cm/s^2 might have occurred during the possible abrupt movement, if we assume constant acceleration lasting from 1 s to 15 min.

PATTERN OF DISPLACEMENT

In order to describe the spatial pattern of movement and its annual variations, the displacements of many points on the surface of the landslide were measured. Analysis of the displacements using a simple kinematic model can show whether mass flux was uniform during an episode of movement and can show the influence of variation in width and thickness of a landslide on the spatial distribution of displacement. The spatial pattern of displacement has been used to identify zones of gross longitudinal stretching and shortening to aid in estimating horizontal stresses in a landslide (Baum and Fleming, 1991). Patterns of displacement also have been used to study landslide mechanisms (Lantz, 1984; Ter-Stepanian, 1984) and the propagation of stress waves in landslides (Iverson, 1986).

Each year from 1983 to 1986, the displacements followed a general pattern of increasing from a small value at the head (near station 0) to a maximum value somewhere near midlength of the landslide and decreasing to a small value at the terminus (pl. F1). Ground upslope from the maximum displacement was stretched longitudinally and

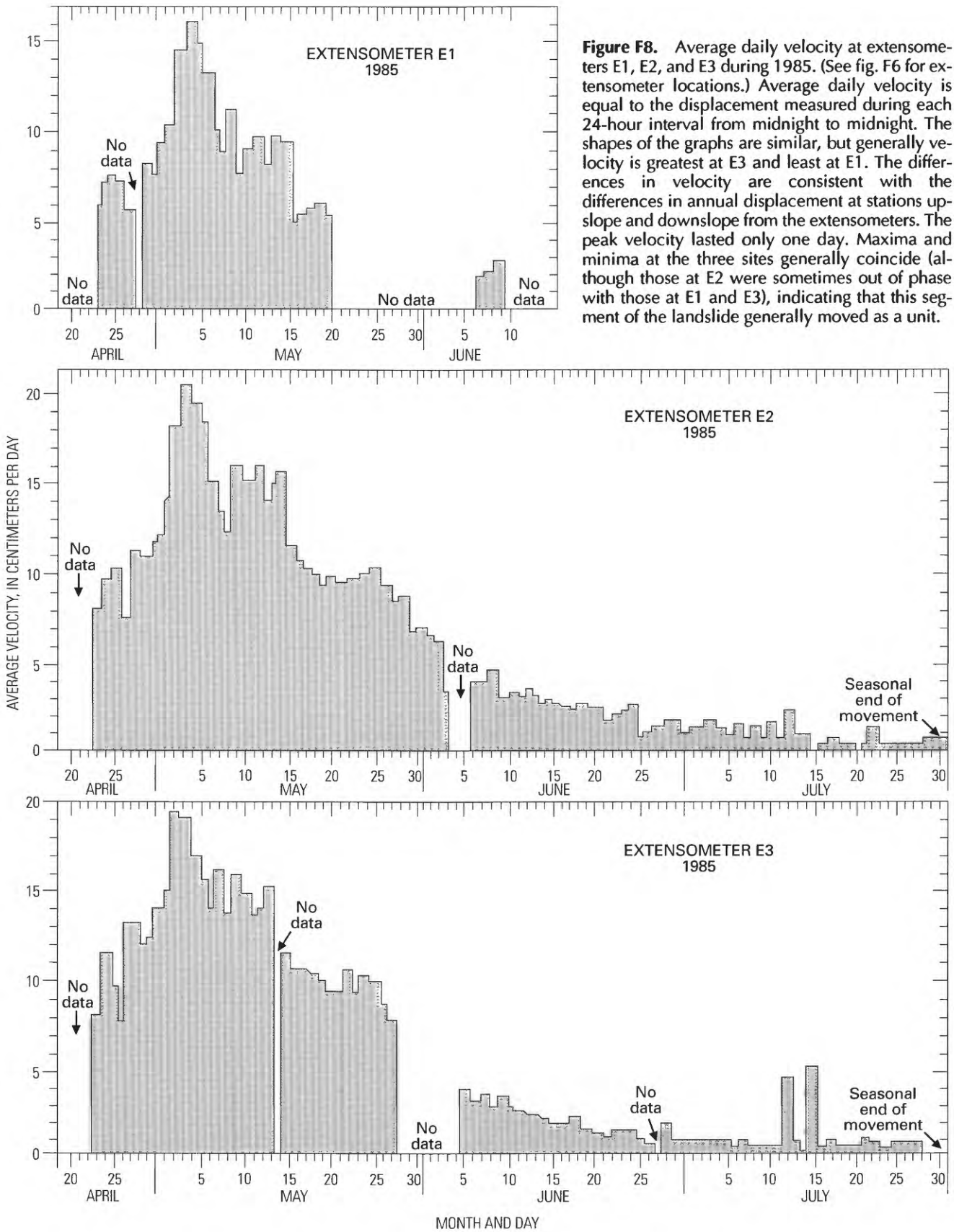

Figure F8. Average daily velocity at extensometers E1, E2, and E3 during 1985. (See fig. F6 for extensometer locations.) Average daily velocity is equal to the displacement measured during each 24-hour interval from midnight to midnight. The shapes of the graphs are similar, but generally velocity is greatest at E3 and least at E1. The differences in velocity are consistent with the differences in annual displacement at stations upslope and downslope from the extensometers. The peak velocity lasted only one day. Maxima and minima at the three sites generally coincide (although those at E2 were sometimes out of phase with those at E1 and E3), indicating that this segment of the landslide generally moved as a unit.

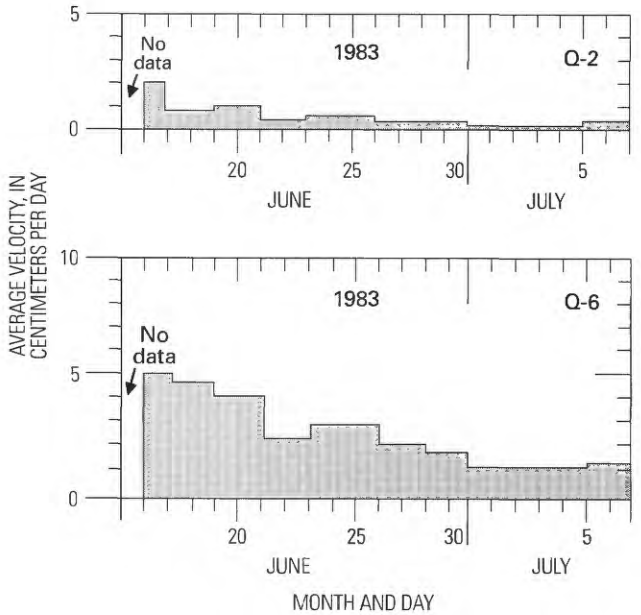

Figure F9. Average daily velocities at quadrilaterals Q–2 and Q–6 during part of 1983. (See fig. F1 for quadrilateral locations.) Quadrilaterals were installed in mid-June 1983 after the rate of movement had already peaked. The shapes of the graphs are almost the same, but the velocity at Q–6 is approximately 2 to 3 times as great as that at Q–2.

ground downslope from the maximum was shortened longitudinally. We have no displacement data for the part of the landslide between stations 425 and 590, but structures produced by the movement indicate that it is also a zone of shortening. The same general pattern of displacement was observed in 1983, 1984, 1985, and 1986; thus, the cumulative longitudinal strains have increased each year.

An inverse relationship between the width and annual displacement is evident in part of the landslide, particularly between stations 120 and 760 (pl. F1). The largest displacement occurs in a narrow part of the landslide, and the displacements decrease upslope and downslope, where the landslide is wider. The apparent inverse relationship is consistent with the principle of conservation of mass. If the mass flux of landslide material is constant, then a simple form of the continuity equation indicates that the displacement, d, should be inversely proportional to the area of a transverse cross section of the landslide, A (A depends on the width), at the station where the displacement is measured. Thus,

$$d_1/d_2=A_2/A_1, \qquad (1)$$

where the subscripts refer to any two stations along the length of the landslide.

Equation 1 is based on assumptions that density is constant, that thickness is independent of time, and that surface displacements are equal to displacements averaged

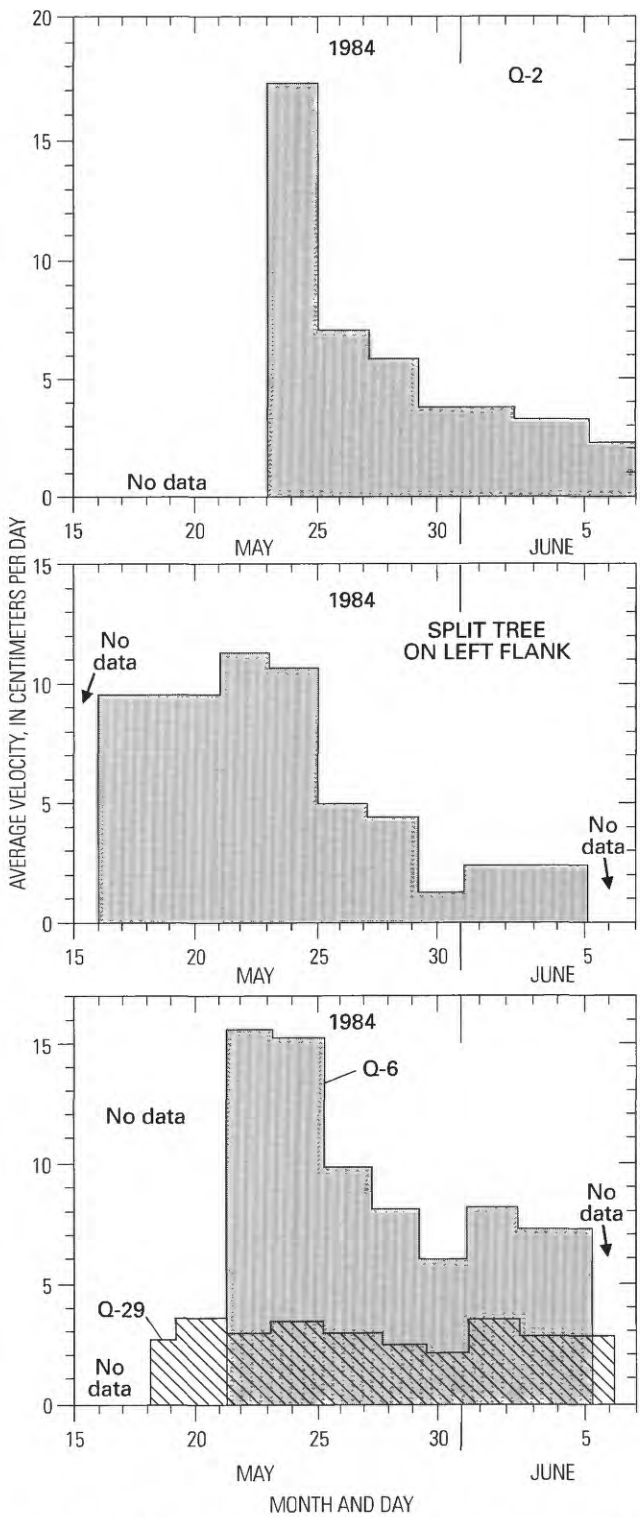

Figure F10. Average daily velocities at quadrilaterals Q–2, Q–6, and Q–29 (fig. F1) and at the split tree on the left flank (pl. F1) during part of 1984. The velocity upslope from Q–2 peaked sometime between May 17 and May 21. The net slip at the road above Q–2 was 1.6 m during this 4-day interval, so the average velocity then must have been 40 cm/d, and the peak was probably greater. The differing shapes of these graphs show that movement during 1984 was less uniform than in 1983 (fig. F9).

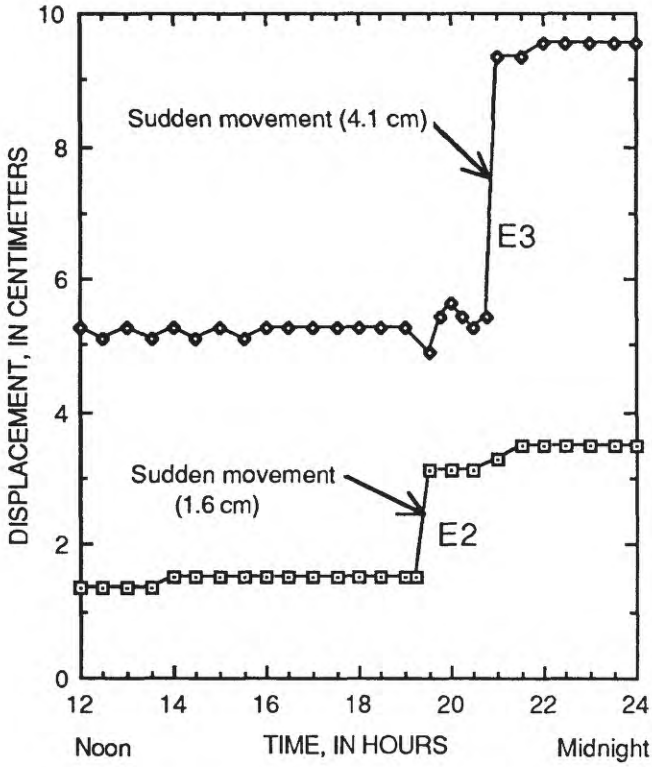

Figure F11. Displacements at extensometers E2 and E3 on the evening of July 13, 1985. The landslide was creeping a few millimeters per day except for the sudden movements indicated by abrupt vertical shifts in the lines of data points. A sudden movement of 1.6 cm was registered at E2 between 7:15 and 7:30 p.m. Later, between 8:45 and 9:00 p.m., a sudden movement of 4.1 cm was registered at E3, about 60–70 m downslope from E2 (fig. F6).

over the thickness of the landslide. These assumptions do introduce some errors, but they are not great enough to completely mask the gross pattern of displacement due to variation in the cross-sectional area of the landslide. Although bulk density of the landslide material does not vary much from place to place, it may decrease slightly due to movement. We know that the thickness changed by a few percent in most parts of the landslide and by as much as 30 percent in some places during four years of movement. Thus, the assumption of constant thickness introduces significant error locally. Surface displacements are greater than displacement averaged over the thickness. However, velocity profiles of other similar landslides indicate that the difference is generally less than 10 percent (Ter-Stepanian, 1965; Rybář, 1968; Skopek and others, 1972; Keefer and Johnson, 1983; Van Asch and Van Genuchten, 1990).

Despite annual repetition of the general pattern of displacement, the flux of landslide debris was nonuniform and not truly steady. Equation 1 predicts that the ratio of displacements at any two cross sections is constant through time if the flux is constant. The displacements shown on plate F1 have been divided by the displacement at line M (normalized) and replotted in figure F12. The normalized displacements follow a general pattern determined by the variable width and thickness of the landslide (fig. F12, pl. F1) consistent with equation 1. If we had sufficient data on thickness of the slide, we could have predicted the normalized displacement for steady movement using equation 1. The normalized displacements would have been constant from year to year had the movement been truly steady. Temporal deviations from the general pattern result from localized deformations, such as rapid evolution of the head during 1984, development of the scarps near station 180 from 1984 to 1986, thickening near station 380 from 1983 to 1986, and enlargement of the terminus of the landslide from 1983 to 1985 (pl. F1).

In 1983, the terminus was poorly defined; cracks marking the flanks of the landslide were visible in the ground surface only as far downslope as station 600. The landslide enlarged in 1984 by propagating cracks downslope to the pipeline, but no cracks were present beyond that point. In 1985, however, cracks could be traced downslope from the pipeline for about 100 m to small toes that were apparently the downslope limit of displacement. Based on observations of similar features in areas where we had displacement data, the cracks and small toes probably represent 20 to 30 cm of displacement where no evidence was observed in 1984. Enlargement of the terminus is reflected in the increase of displacements downslope from station 600 between 1983 and 1985 (fig. F12, pl. F1).

DISTRIBUTED SHEAR WITHIN THE LANDSLIDE DEBRIS

A purpose of the transverse stake lines was to determine how displacement was distributed across the width of the landslide (fig. F13). Specifically, we wanted to determine whether the landslide moved by shear concentrated at the boundaries (Keefer and Johnson, 1983), shear distributed across the width of the landslide, or some combination of the two (Harden and others, 1978; Oberste-Lehn, 1976). The stakes within each line moved at different rates relative to their neighbors, and patterns of differential movement developed gradually. Thus, the pattern of differential movement was more obvious at the end of 1986 than in previous years.

Displacement of the transverse lines indicates that the landslide moved primarily by shear concentrated at its boundaries. Displacement of stakes near the boundaries ranges from 82 to 97 percent of the displacement near the axis of the landslide (fig. F13). Distributed

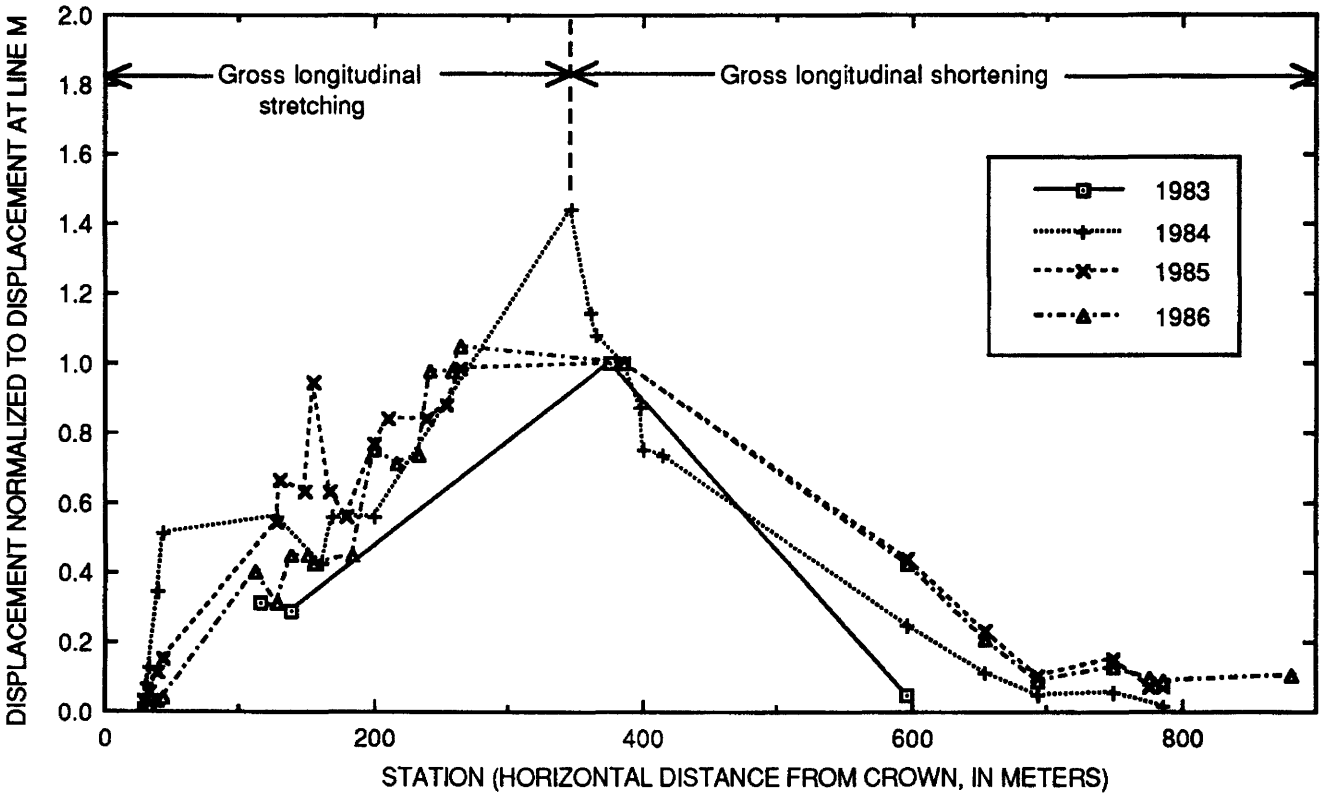

Figure F12. Normalized annual displacement of points at the surface of the Aspen Grove landslide from 1983 to 1986. Station numbers along the horizontal axis of the graph correspond to stations on plate F1 and indicate the distance downslope from the crown. The annual displacements were normalized by dividing them by the displacement for the corresponding year at line M (pl. F1). The maximum displacement occurred between stations 300 and 400. The displacement gradient (slope of the graph) is generally positive upslope from the maximum, indicating gross longitudinal stretching. Gross longitudinal shortening occurred downslope from the maximum, where the slope of the graph is generally negative. The margin of error in determining the annual displacements is generally ±10 cm (about the size of the plot symbols at the scale of the graph).

shear within a few meters of the boundaries accounts for the remainder of the displacement at the axis. The displacement profiles of the transverse lines show evidence of plastic deformation possibly related to convergence or divergence of the lateral boundaries of the landslide, as well as deformation due to bending as the material moves down the slightly sinuous channel of the landslide.

The pattern of displacements in line M is consistent with the pattern of displacement due to bending about a vertical axis outside the left flank of the landslide superimposed on plastic flow in a converging channel with friction at the boundaries (Hill, 1950, p. 208–212). Stakes near the middle of the line M moved farther than points near either flank, and stakes near the right flank moved farther than those at the left flank. Although we model the landslide as a simple plastic here, we expect similar velocity profiles to occur in other materials as well, provided the material is allowed to slip at the boundary. The boundaries of the landslide converge upslope and downslope from line M, making angles of 3.2° with the axis of the landslide. The left flank curves near line M, causing the landslide to turn a few degrees to its left.

The velocity distribution for plastic flow in a straight, converging channel is determined by the following formula (Hill, 1950, p. 211)

$$v_r = \frac{B}{r(c-\cos 2\psi)} \quad ; \quad c>1 \ , \qquad (2)$$

where v_r is the radial component of velocity, B is a positive constant that has dimensions of length squared divided by time, ψ is the angle between the algebraically greatest principal stress and a radial line (ranging from zero at the axis of the channel to $\pi/4$ radians (45°) at the edge of the channel), r is a radial distance measured from the apex of the channel (fig. F14*A*), and c is a positive constant (greater than unity) that depends on α, which is one-half the angle between the sides of the converging channel (fig. F14*A*). The quantity c is graphed as a function of α in figure F14*B*. In deriving equation 2, Hill (1950) assumed that the friction at the boundaries equals the yield strength of the plastic material, but explained how the formula can be adapted if the friction is less than the yield strength.

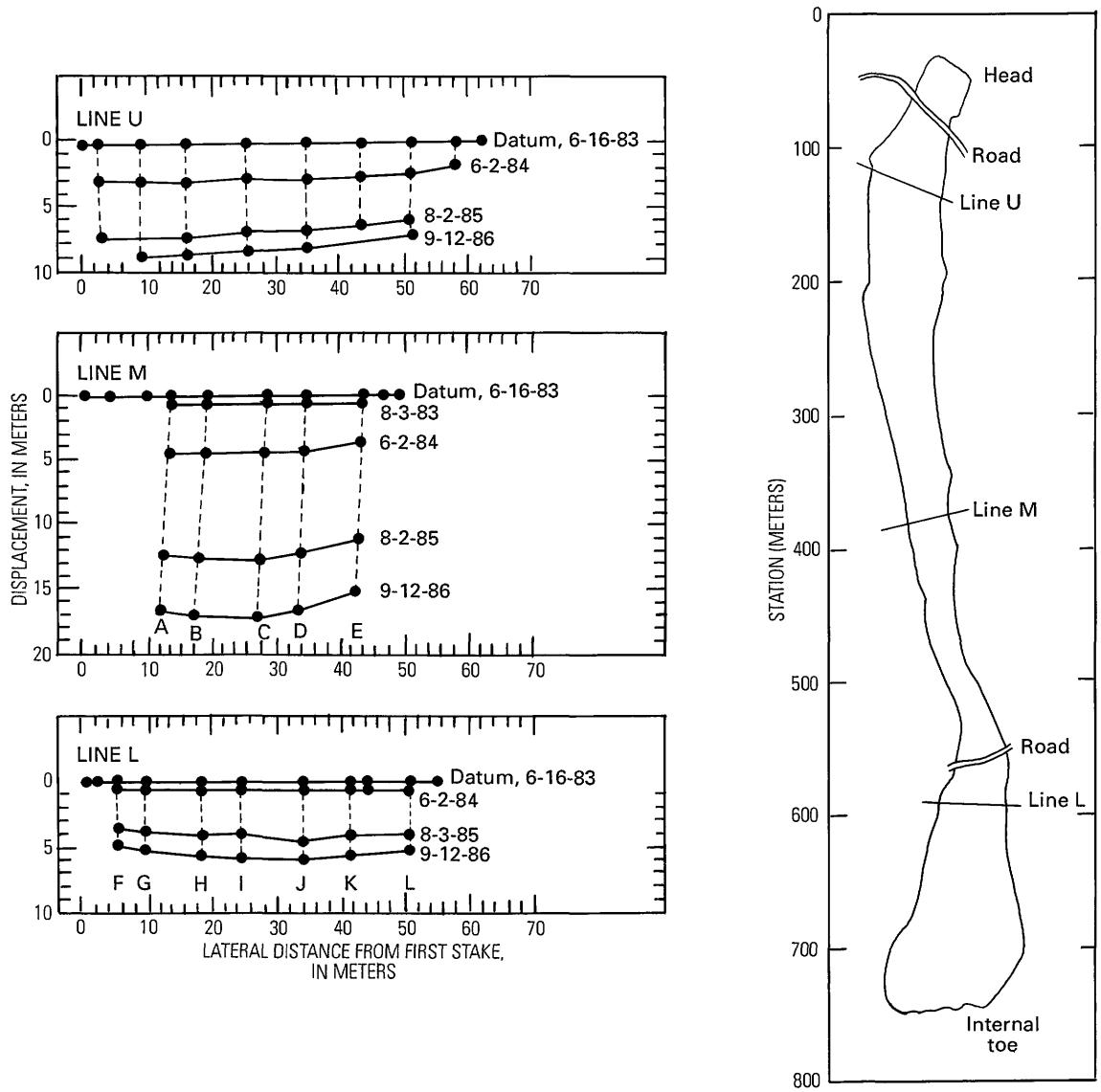

Figure F13. Displacement of transverse lines of stakes in the upper, middle, and lower parts of the Aspen Grove landslide. Solid circles indicate positions of stakes on dates of measurement. Map along the right side indicates location of each line. The greatest displacement occurred near the axis; displacement at the edges is from 3 to 18 percent less than at the axis. Thus, from 82 to 97 percent of movement at the axis results from shear at the boundaries, and the remainder results from distributed shear within the landslide.

The constant B is determined by measuring the velocity at the axis of the channel (where ψ is zero). The radius r at the point where the velocity is measured and c are determined by the geometry of the channel. B is then computed from the following formula:

$$B=v_r r(c-1)\,. \qquad (3)$$

The angle θ between the channel axis and any other radial line in the channel (fig. F14*A*) is related to c and ψ by the following (Hill, 1950):

$$\theta = -\psi + \frac{c}{\sqrt{(c^2-1)}}\tan^{-1}\left\{\sqrt{\left(\frac{c+1}{c-1}\right)}\tan\psi\right\}\ ;\ c>1. \qquad (4)$$

θ takes on values between 0 and α. At line M, α is 3.2°, and the corresponding value of c is 9.5 (fig. F14*B*).

Figure F15*A* compares the velocities predicted by plasticity theory for a straight converging channel having friction at its boundaries with the displacements of points in line M between 1983 and 1986. Points in line M to the

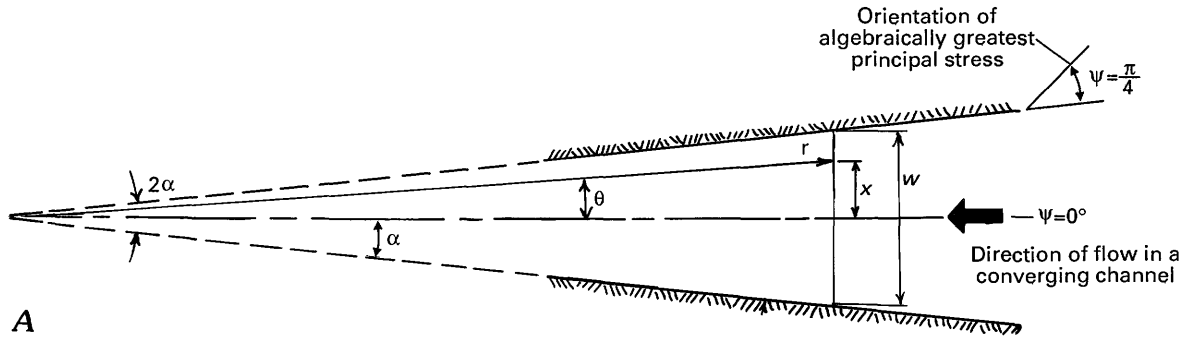

A

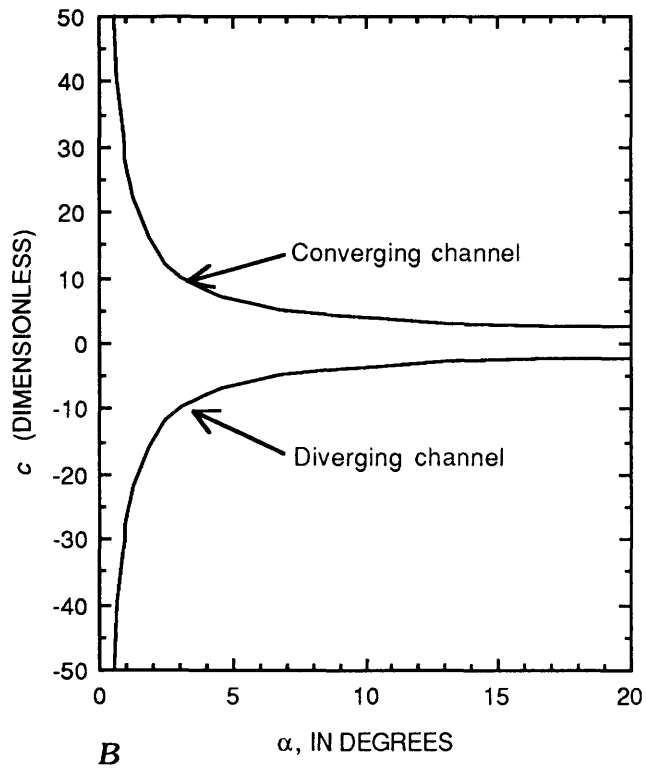

B

Figure F14. Parameters used in analysis of flow in converging and diverging channels. *A*, Sketch showing a converging or diverging channel. α is the acute angle between the axis and the side of the channel, θ is the angle between the axis and any radial line in the channel, ψ is the angle between the algebraically greatest principal stress and any radial line, *r* is the radius measured from the apex of the channel, and v_r is the velocity parallel to any radius in the channel; v_r is positive for movement in a converging channel (toward the apex). *B*, Graph showing the constant *c* (equations 2–6) as a function of α for movement in converging and diverging channels.

right of the axis of the slide plot above the theoretical velocity profile for plastic flow in a straight, converging channel, and points to the left plot below the curve. However, the points are near the curves for a velocity profile in a converging channel that bends slightly to the left of an observer facing downslope.

The pattern of displacements in line L is consistent with plastic deformation in a diverging channel having friction at its boundaries. The velocity is greatest at the axis of the channel and decreases toward the channel boundaries, just as predicted by Hill's (1950) theory for flow in a diverging channel. This theory is summarized by formulas similar to equations 2 and 4. The velocity is determined by the following equation:

$$v_r = \frac{B}{r(c+\cos 2\psi)} \quad ; \quad c<-1. \qquad (5)$$

The variables in equation 5 have the same definitions as in equation 2, except that *c* is a negative constant less than –1, because the shear stress at the wall of the channel acts in the opposite direction of that for converging channel flow. (This change in the definition of *c* is not obvious from the discussion in Hill, 1950, p. 212.) At line L, α is approximately 9°, and the corresponding value of *c* is –3.983 (fig. F14*B*).

The angle θ for flow in a diverging channel is determined by

$$\theta = \psi - \frac{c}{\sqrt{(c^2-1)}} \tan^{-1}\left\{-\sqrt{\left(\frac{c-1}{c+1}\right)}\tan\psi\right\} \quad ; \quad c<-1. \qquad (6)$$

In equation 6, ψ ranges from 0 at the axis of the channel where θ=0, to –π/4 radians (–45°) at the edges of the channel, where θ=α.

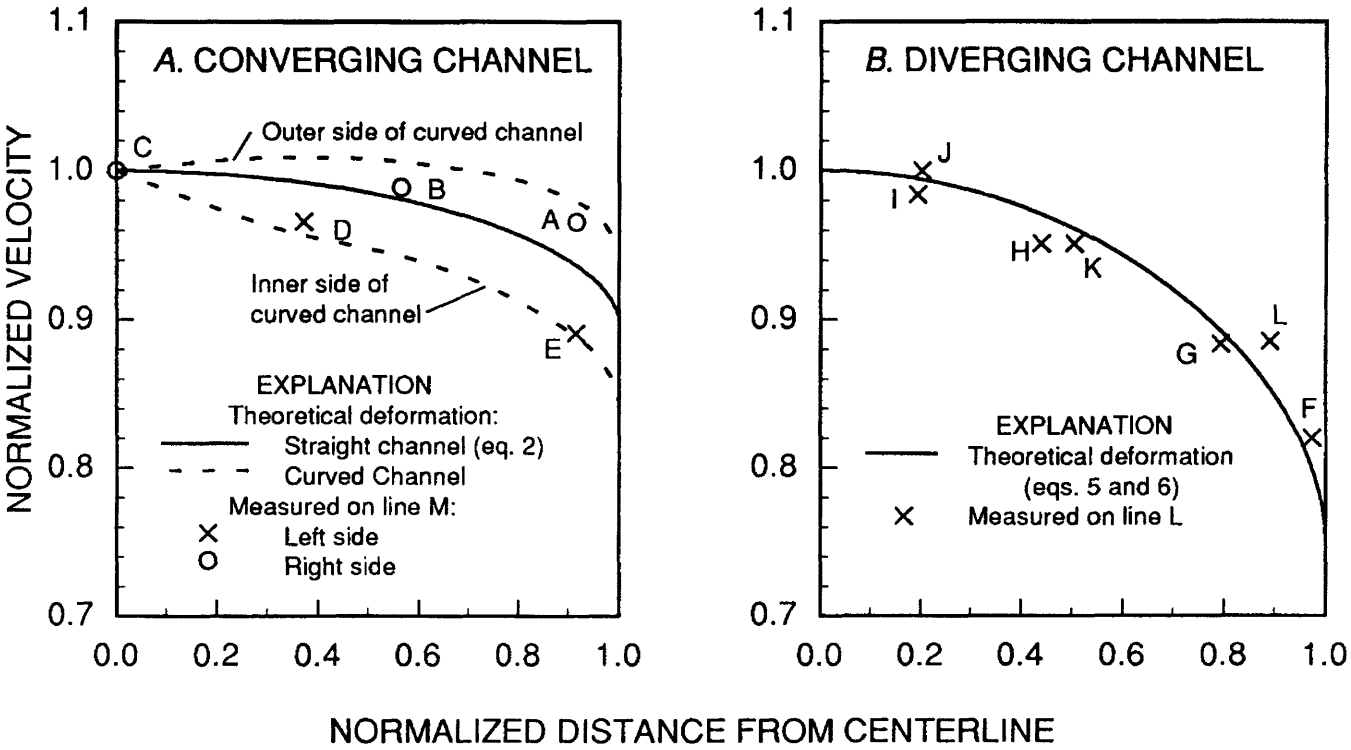

Figure F15. Observed deformation at transverse lines of stakes compared to theoretical plastic deformation in converging (*A*) and diverging (*B*) channels. Capital letters designating stakes correspond to those shown in figure F13. "Normalized distance from centerline" (x/w in fig. F14*A*) equals $\sin\theta/\sin\alpha$. "Normalized velocity" represents the cumulative displacement of each point from 1983 to 1986 divided by the displacement of points at the axis of the landslide. Displacements were measured by plane-table mapping and have a margin of error less than ±10 cm, which is too small to show on these plots. Theoretical velocity profiles for flow in straight channels with friction at the boundaries are based on equation 2 (for converging channel) and equation 5 (for diverging channel). Profiles shown in *A* for a curved channel are based on the assumption that bending of a few degrees causes a linear gradient in the velocities of points across the channel, as in the bending of beams (Popov, 1968). The gradient results in higher velocities for particles on the outer side of the bend (in this case, the right side of the channel) and lower velocities for those on the inner (left) side.

Figure F15*B* compares normalized velocities predicted by the theory for plastic flow in a diverging channel (equations 5 and 6), with normalized displacements of stakes in line L for the period from June 1983 to August 1986. The normalized displacements of stakes plot slightly above or below the theoretical curve in figure F15*B*. Thus, the theory predicts velocities in line L with fair accuracy, and there is no evidence for bending as in line M.

Although Hill's (1950) model for plastic deformation is able to predict qualitatively the displacement profiles at lines M and L, several assumptions may limit its applicability to landslides. The deformation in the landslide is three-dimensional, whereas the model is for plane deformation. The landslide material is a bouldery clay, which probably does not deform as an ideal plastic. In fact, deformation of the landslide material might be localized on shear surfaces rather than being distributed as in the model. We lack needed data to determine whether the deformation is localized on several minor shear surfaces or distributed. One prediction of the model that we were unable to verify, but consider unlikely, is constant velocity (plug flow) through a section of channel having straight, parallel sides.

Models of flow for viscous fluids in channels of various shapes yield profiles that are superficially similar to those predicted here (Nye, 1965). However, in most fluid models, the velocity at the boundary is assumed to be zero, rather than a finite value as assumed in the model for plastic deformation and as observed in the field.

At line U, displacement was greatest near the right flank and least near the left flank (fig. F13). Left-lateral shearing parallel to the direction of movement and distributed across the entire width of the landslide could account for the observed gradient in displacement. Bending of the landslide to the left could also account for the observed gradient.

We cannot determine which style of deformation occurred at the line U. Bending would cause compression

near the left flank and elongation near the right flank, but presumably, distributed shearing would not produce such compression and elongation. Although a thrust fault, which indicates compression, is mapped next to left flank near line U (fig. F1), no corresponding evidence of extension was present along the right flank near line U. In fact, longitudinal shortening ranging from 1 to 6 percent occurred at Q–4, which is right of center along line U. Aspen trees in a cluster along line U remained upright even though they were transported nearly 10 m. Large inhomogeneities in the deformation would have disturbed the trees.

LOCALIZED DEFORMATION

Deformation associated with geologic structures on the surface of the landslide was documented by a combination of plane-table mapping and repeated measurements of quadrilaterals and stake lines; these measurements facilitate modeling the formation of several kinds of structures on the surfaces of landslides. Parts of the landslide were mapped each year during August to record changes in the structures. Strain and tilt were computed from the quadrilateral measurements, and strain was computed from stake-line measurements.

The following sections describe the evolution of structures in zones of longitudinal stretching and shortening (Baum and others, 1989), formation of a flank ridge, and deformation over a bump in the slip surface. These kinds of deformation are common on many landslides, and their identification has practical value. Horizontal stresses approach their minimum values (active earth pressure) in zones of longitudinal stretching, and approach their maximum values (passive earth pressure) in zones of longitudinal shortening. Identification of bumps and depressions in the ground surface of a landslide that mimic bumps and depressions in the slip surface helps determine the shape of the slip surface. Discovering the origin of flank ridges may eventually lead to insights into processes within active landslides and help explain the formation of analogous ridges adjacent to strike-slip faults (Fleming and Johnson, 1989).

Deformation in Ground Being Extended

The sequence of deformations in ground being extended was observed at two places in the Aspen Grove landslide. The head of the landslide began to develop in 1983 but evolved rapidly during 1984; only late stages of its development were recorded. The second area of ground being extended was in the "pond" segment of the landslide (pl. F1) where a group of scarps formed between 1984 and 1986. The scarps developed slowly over the three seasons, and early stages of their development were observed and documented. In order to describe the sequence of deformations that occur in ground that is being extended, the development of the scarps is described first; subsequently, the late-stage development of the head is described.

The scarps.—The scarps are in the upper part of the landslide, near station 170 (pl. F1). This part of the landslide is about 64 m wide, and strike-slip faults parallel to the flanks divide it into three elements (fig. F16*A*). The central element, where the scarps formed, is 46 m wide. Ground on the distal side of the group of scarps slopes about 12° toward the northwest. Ground on the proximal side of the scarps has a back slope of about 6° toward the north-northeast.

During 1983 and the early part of 1984, the ground at the site of the scarps was undeformed. No cracks had formed there, and quadrilateral Q–5, which was at the site (fig. F16*A*), showed no significant changes.

Early stages of extension were evidenced by changes in the ground surface and deformation at quadrilateral Q–5 during 1984. By the end of 1984, two sets of cracks had appeared at the site (fig. F16*A*). The cracks had rough, irregular surfaces consistent with opening in tension. Deformation at Q–5 during 1984 was consistent with displacement on a normal fault between stake *B* and the other stakes in Q–5 (Baum and others, 1988, p. B17).

Evidence of stretching became more pronounced during 1985. The cracks that had formed in 1984 enlarged and new cracks appeared (fig. F16*B*). The upper group of cracks occupied about the same position as in 1984, but the cracks were larger and defined a crescent. The lower group of cracks extended across the entire width of the central landslide element.

By September 1986, scarps had formed in the left half of the central landslide element. The upper, crescent-shaped group of cracks evolved into a family of normal faults (fig. F16*C*), which formed the group of scarps. New cracks formed and older cracks enlarged.

The head.—A few small cracks defined the head of the landslide in June 1983. The cracks were oriented approximately perpendicular to the axis of the slide, and the highest cracks were at about the 2,420-m contour (fig. F1). The flanks in the head area were marked by small en echelon cracks. Measurements at quadrilateral Q–1 indicated that ground at the head accommodated at least 3 percent elongation before the cracks appeared.

The head evolved rapidly between May 17 and May 21, 1984. On May 17, the head was concealed by several inches of snow, and the road across the landslide just below the head was still intact. On May 21, most of the snow had melted and gaping cracks had appeared. Displacement at the uppermost crack in the head was 0.3 m, and displacement increased downslope in the head region. The cracks were about 1 m deep and separated the head into a group of irregular blocks (fig. F17). The flanks

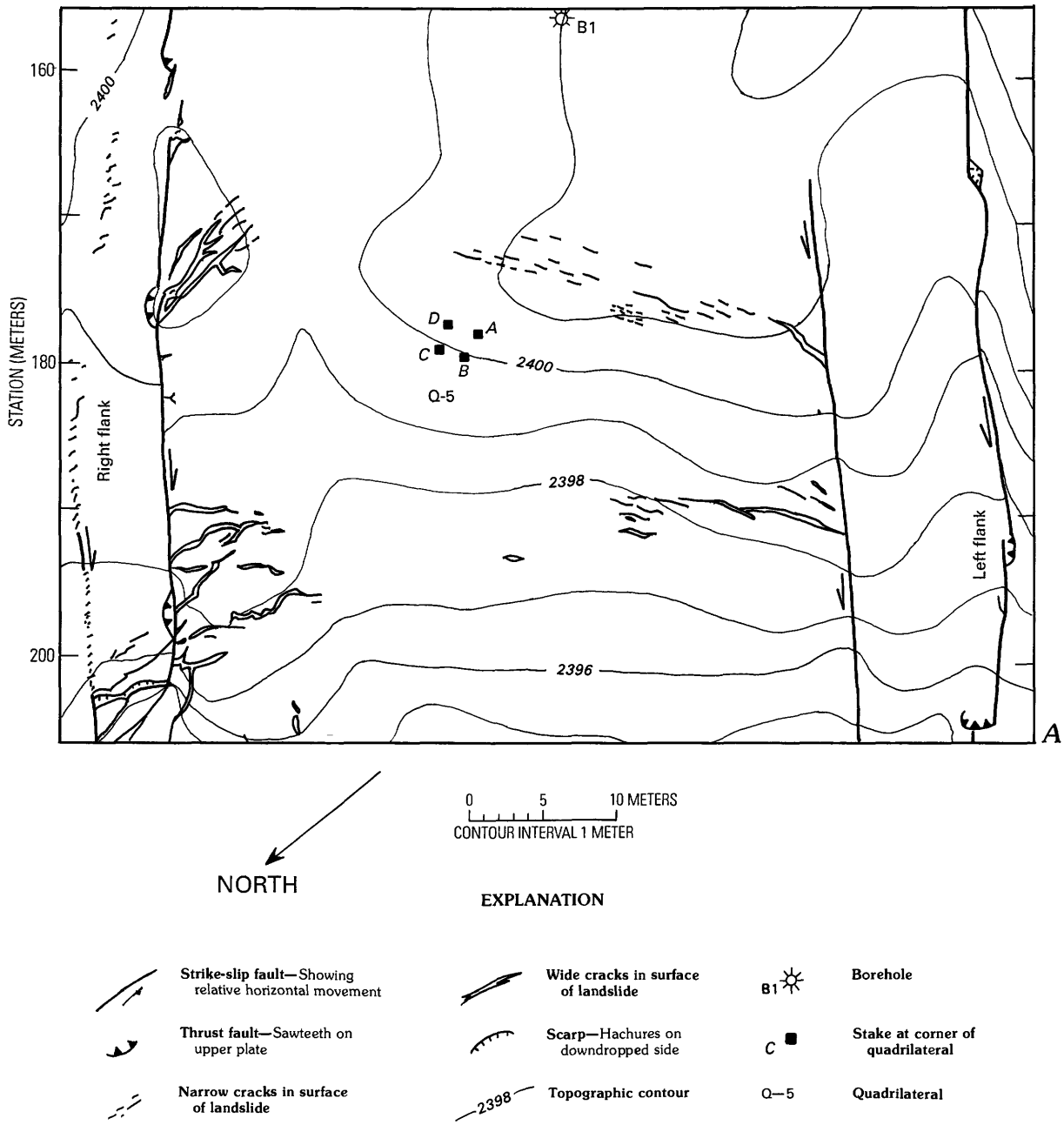

Figure F16 (above and facing page). Plane-table maps of the landslide near station 170 showing the development of scarps in ground that was stretching longitudinally. See figure F1 for location of map area. *A*, August 1984. Two sets of narrow cracks formed transverse to the axis of the landslide during the summer of 1984. An upper set appeared near the 2401-m contour and a lower set at the 2398-m contour. *B*, August 1985. The upper set of cracks enlarged and became more arcuate, and a crack appeared inside Q–5. Cracks in the lower set increased in size and number, and the lower set extended across the full width of the slide. *C*, September 1986. Many of the cracks in the upper set evolved into arcuate, downhill-facing scarps. Cracks in the lower set near the right flank enlarged greatly during 1986.

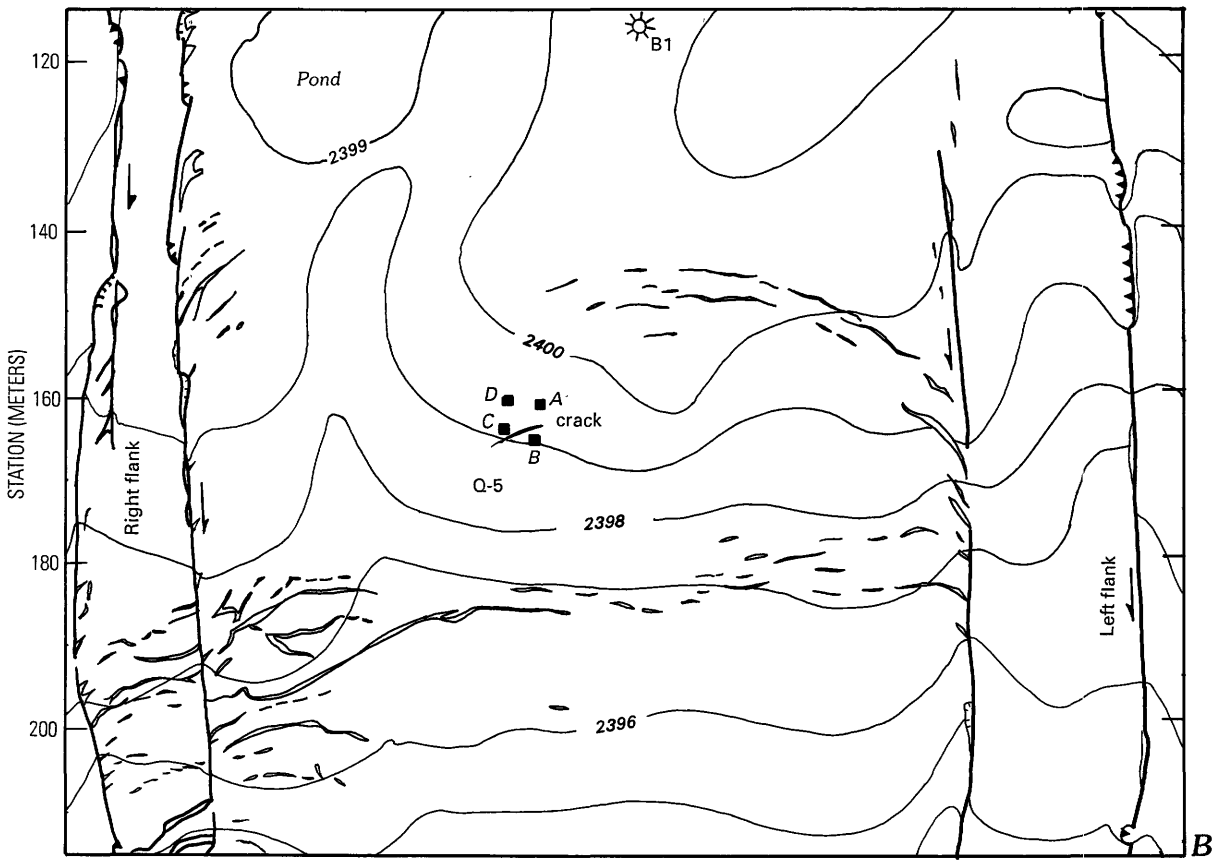
120
140
160
180
200
STATION (METERS)
Pond
B1
2399
2400
D
A
C
crack
B
Q-5
2398
Right flank
Left flank
2396
B

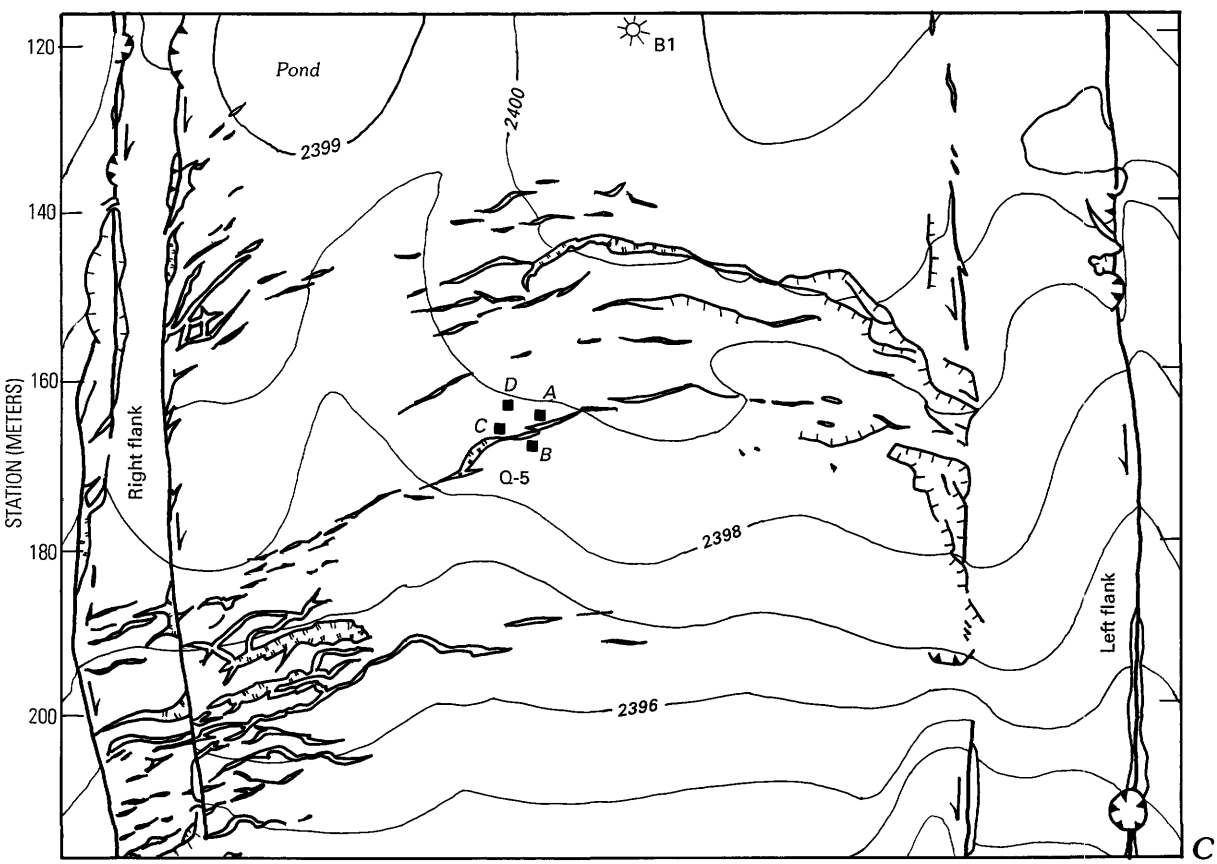
120
140
160
180
200
STATION (METERS)
Pond
B1
2399
2400
D
A
C
B
Q-5
2398
Right flank
Left flank
2396
C

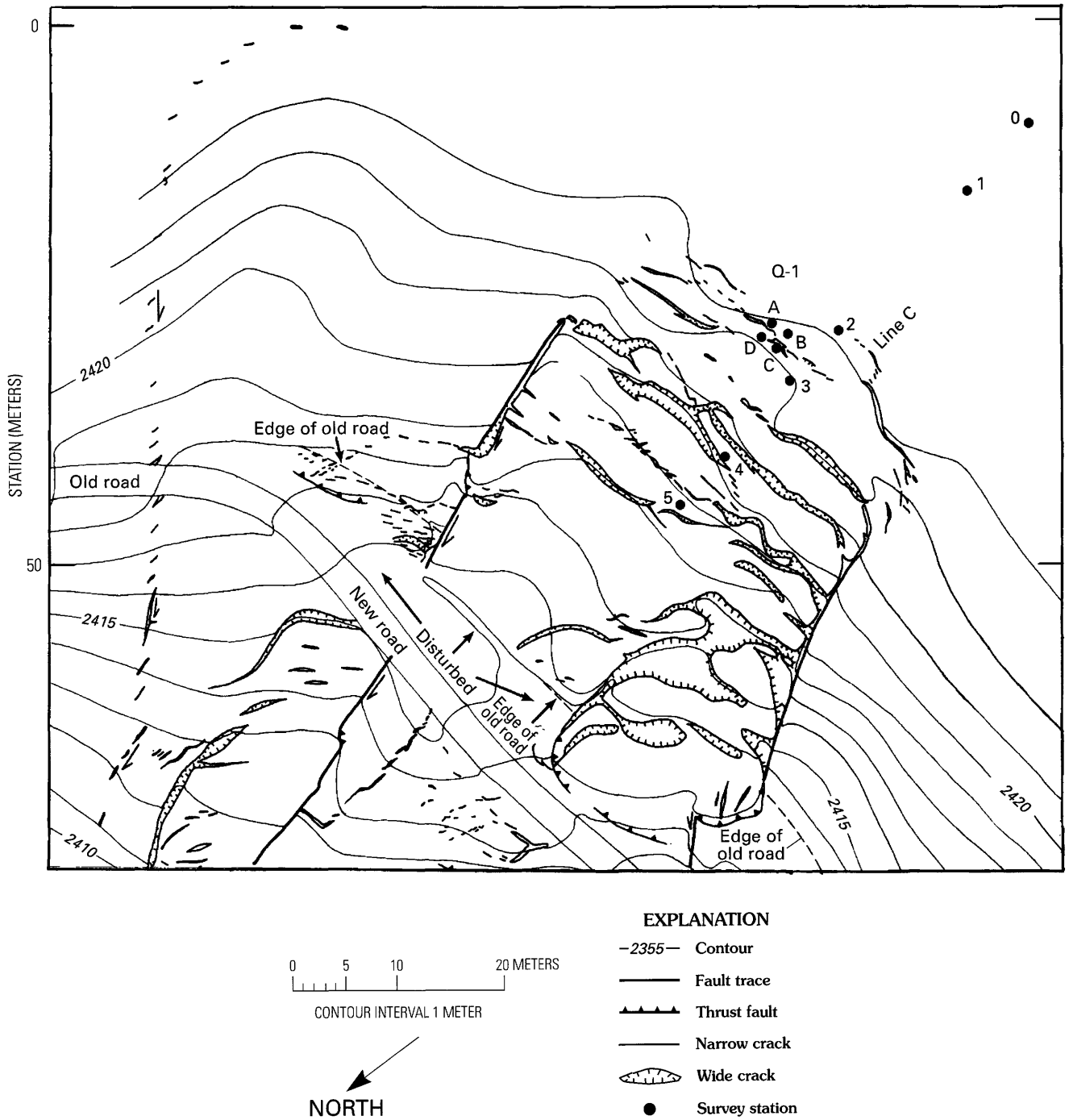

Figure F17. Plane-table map showing the head of the Aspen Grove landslide, August 1984. See figure F1 for location of map area. The head represents a late stage of development of ground being stretched. Gaping tension cracks, transverse to the flanks of the landslide, about 1 m deep and as much as 1 m wide, formed as the head stretched during a period of rapid movement in the middle of May 1984. A group of tension cracks, shaped like an inverted *J*, formed later in May, as an apparent precursor to further enlargement of the head.

of the landslide had evolved into strike-slip faults, and the road was offset about 1 m vertically on the left flank. The head may have moved more rapidly than any other part of the landslide; it apparently moved at least 40 cm/d.

The head slowly enlarged during the remainder of 1984 and during 1985. A group of en echelon cracks that outline an inverted *J* formed east of the head during late May of 1984 (fig. F17). En echelon cracks constituting an upslope extension of the left flank formed during 1985 (pl. F1). Displacement measurements upslope from the head along line C (fig. F17) showed +0.6 percent of axial stretching during 1984, before the en echelon

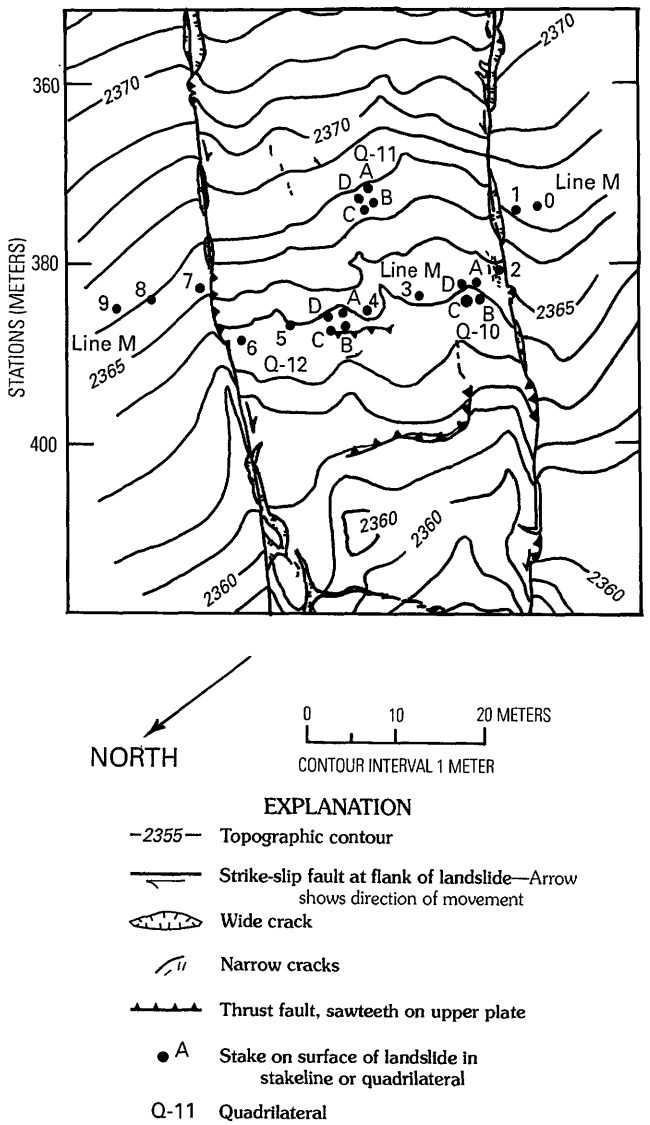

Figure F18. Plane-table map showing topography and structures in ground near line M (station 390) that was shortening longitudinally in August 1984. See figure F1 for location of map area. In 1984, scarps 1.0–1.5 m high defined the right flank and scarps 0.5–1.0 m high defined the left flank. The scarps were only 0.3 m high when first observed in June 1983. By the end of 1986, scarps at the right flank were 1.5–2.0 m high and those at the left flank were 1.0–1.5 m high. Contraction of the quadrilaterals and the formation of thrust faults, one at the 2361-m contour and another next to Q–12, indicate that this part of the landslide was being shortened.

cracks appeared, and another +0.8 percent as the cracks formed in 1985.

Deformation in Ground Being Shortened

Detailed measurements of quadrilaterals documented the deformation of two areas that shortened axially. These areas are the vicinity of line M, between stations 370 and 400, and the large internal toe, between stations 600 and 760. Measurements indicate that ground in the vicinity of line M thickened. The internal toe thickened and grew in height.

Thickening between stations 370 and 400.—The ground surface of the landslide grew in height from 1983 to 1986. The surface was elevated 0.3 m relative to ground neighboring the landslide between stations 220 and 420 in August 1983, and the left flank became more elevated between 1983 and 1986. Buckles and small thrust faults formed at the ground surface (fig. F18). This entire section of the landslide also narrows uniformly from 55 m at station 225 to 30 m at station 420.

Deformation of quadrilaterals near line M indicates that the landslide thickened nonuniformly between 1983 and 1986. Quadrilateral Q–11 and triangle *BCD* of Q–12 (fig. F18) contracted between June 1983 and September 1986. Stake A of Q–12 was disturbed in 1985, so we have incomplete data for the remaining triangles in Q–12. The final areas of the triangles in Q–11 ranged from 82 to 85 percent of their initial areas, and the final area of triangle *BCD* in Q–12 was 77 percent of its initial value. Contraction of the quadrilaterals indicates that the landslide thickened 18 to 23 percent beneath Q–11 and 30 percent beneath Q–12, assuming that the bulk density of the landslide was constant. The ratio of the final volume to the initial volume of slide material beneath Q–12 was unity (assuming constant density), and so the ratio of the final thickness to the initial thickness of the slide beneath Q–12 must have been 1/0.77=1.3 (Malvern, 1969, p. 167; Lantz, 1984).

Thickening can explain the formation of scarps along the flanks of the landslide. The original thickness of the landslide was about 6 m (Baum and Fleming, 1989, p. C5), so the final thickness was between 7.1 and 7.8 m. The difference in the final and the original thicknesses of the landslide, 1.1 to 1.8 m, is consistent with the heights of the scarps, 1.5–2.0 m high on the right flank and 1.0–1.5 m high on the left flank. However, displacement of the landslide can also account for part of the height of the scarps if the original thickness varied along the length of the landslide.

Similar deformation occurred throughout the downslope half of the landslide, although thickening seemed most pronounced near line M. Small thrust faults and buckle folds were fairly common in parts of the landslide being shortened. Thickening was also evident in the increase in height of the internal toe near station 760 (Baum and others, 1988).

Deformation at a Flank Ridge

Flank ridges are low ridges having rounded profiles that form within moving landslide debris on the flanks of

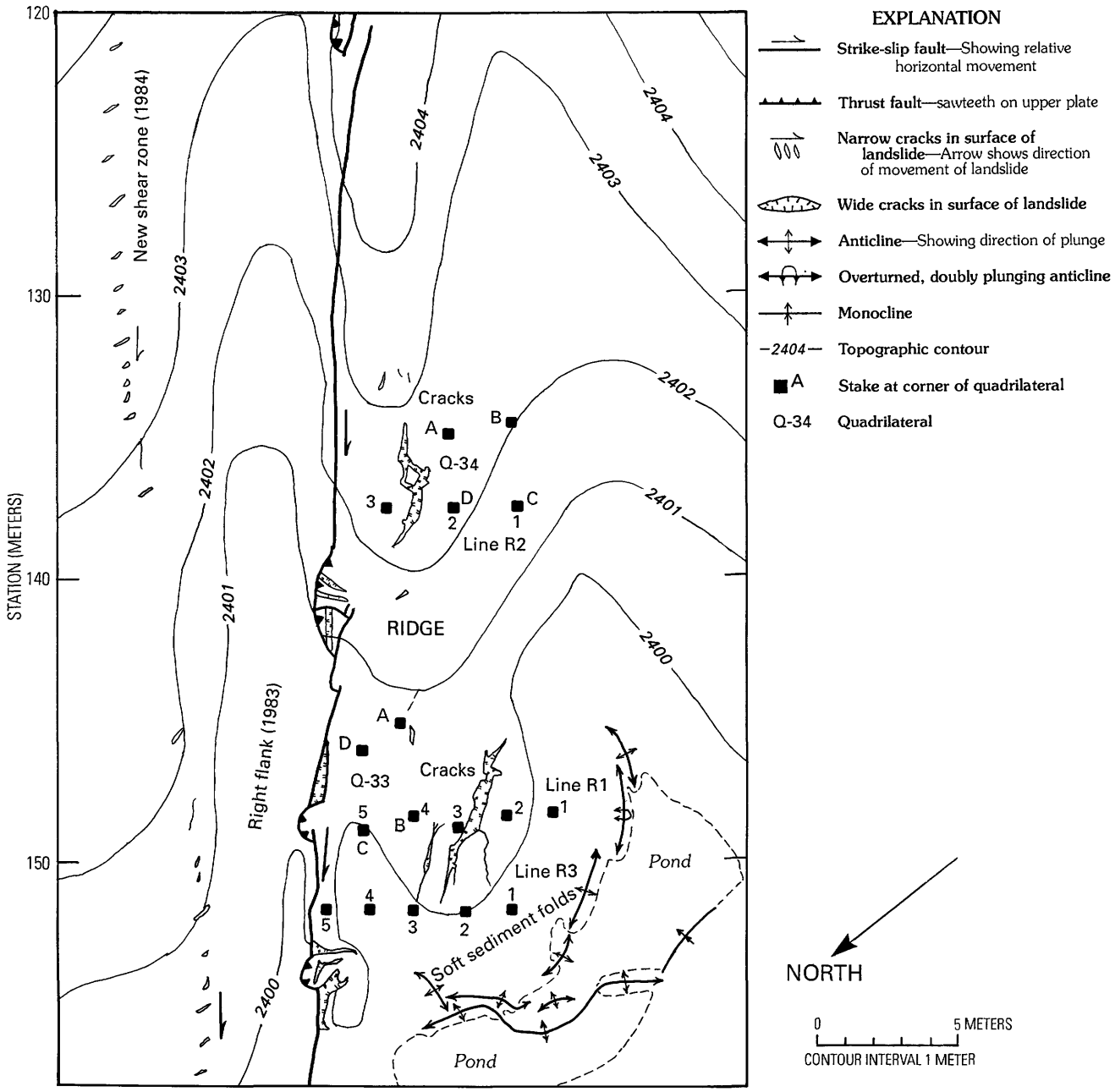

Figure F19. Plane-table map of a flank ridge near station 150 in August 1984, showing topography, cracks, and positions of stakes. See figure F1 for location of map area. The cracks in the crest of the ridge and the soft-sediment folds, which appeared during the spring of 1984, indicated that the ridge might be growing in height.

landslides (Fleming and Johnson, 1989). The ridges are tens of meters long, several meters wide at the base, and from 1 to 4 m high. Flank ridges might be formed by several different modes of deformation. Some ridges outside the margins of the Manti landslide appear to have formed by deposition as the landslide spilled out of its channel. Various kinds of ridges along the flanks of landslides have been described or mentioned in the literature (Hadley, 1964, p. 125–127; Zaruba and Mencl, 1982, p. 79–81, 93, and 150; Crozier, 1984, p. 132–133; Fleming and Johnson, 1989). We also have observed flank ridges on several other landslides in Utah and Colorado. However, little seems to be known about their origins. The kinematics of one ridge is described here.

Observations made in June 1984 of a flank ridge on the right flank of the Aspen Grove landslide, near station 150 (pl. F1), indicated that the ridge might be growing: cracks were present in the top of the ridge (fig. F19). The trunk of a dead tree had been lifted out of the indentation made by the tree on the surface of the ridge.

Based on these observations, quadrilaterals (Q–33 and Q–34) and transverse lines of stakes (R1 and R2) were placed on the ridge early in June 1984 to determine whether it would grow during the summer of 1984. The ridge was mapped during August 1984 (fig. F19). In April 1985, more measurement stations were installed (line R3), and we continued monitoring during the spring and summer of 1985.

Differential vertical displacements of each stake in lines R1 and R2 revealed that the ridge was indeed growing in height and its sides were steepening (fig. F20). Stakes near the crest of the ridge were displaced downward less than stakes on the sides of the ridge. Even though all stakes were moving downward, because the landslide itself was moving downslope, stakes on the crest of the ridge moved upward relative to stakes on the sides of the ridge.

Our observations and measurements place constraints on how the flank ridge formed, but details of the process are still poorly understood. The shear zone that formed at the flank of the landslide in 1983 is about 2–4 m northeast of the crest of the ridge. Another shear zone, 9 m northeast of the ridge crest, began forming in 1984. The height of the ridge increased with displacement even after displacement on the later shear zone became greater than displacement on the 1983 shear zone next to the ridge (fig. F21). The greatest growth in height did not occur at the topographic axis of the ridge (fig. F22*A*). Points on the surface of the ridge were displaced along trajectories that diverge from the 1983 right flank at angles of 5°–10° (fig. F22*B*, table F3), but no evidence of dilation was observed in the right flank. The ridge elongated and sheared parallel to the direction of displacement (fig. F22*B*). The central part of the ridge, which was growing in height, also expanded laterally, but the sides of the ridge contracted normal to the axis of the ridge, so net change in the width of the ridge was negligible (fig. F23).

These observations rule out buckling as a possible mechanism for forming the ridge. The ridge has the shape of a fold, but it did not form as a result of buckling, because net shortening across the ridge (4 cm at lines R1 and R2) was insignificant when compared to the growth in height of the ridge (approximately 12 cm; figs. F20 and F23). The ridge was growing in height even at times when transverse lines across the ridge were stretching (figs. F21 and F23).

Our observations also seem to rule out helical flow as a mechanism for forming this ridge, even though the orientations of the displacement vectors (fig. F22*B* and table F3) seem consistent with the type of helical flow that occurs in some nonlinear fluids (Truesdell, 1964; Rivlin, 1964; McTigue and others, 1985). A qualitative comparison of our observations of the ridge with a model for helical flow (McTigue and others, 1985) indicates that the growth of this ridge differed significantly from the growth of ridges by helical flow. If particles in a growing ridge move along helical paths, the particles on the right flank should circulate in a counterclockwise sense, as viewed from upslope. Particles following such paths would move up next to the fault and subsequently move toward the axis of the landslide, where particles would be moving down toward the slip surface (fig. F24). However, this model does not satisfactorily explain the stretching observed near the axis of the ridge with attendant shortening on the flanks. Furthermore, the helical flow model seems to predict maximum growth in height at the flank (McTigue and others, 1985, p. 125), rather than a few meters inside the flank (fig. F20).

Intrusion of clay beneath the ridge seems the most likely explanation for its growth. The coincidence of transverse stretching and growth in height near the axis of the ridge seems consistent with intrusion of material into the core of the ridge (fig. F25). Models for intrusion generally predict growth in height that is maximum over the center of the intrusion, and gradually decreases to zero some distance beyond the edges (Mogi, 1958). These models also predict that the ground will stretch horizontally above the intrusion and shorten beyond the edges of the intrusion. The vertical displacements agree in general form with the theory (fig. F25). The horizontal displacements are less than predicted by the theory, because of shortening across the ridge (fig. F25). Some of the differences between the theory and observations may also be due to the sparseness of the stakes, localized plastic deformation (cracking) at the ground surface, and idealizing the intrusion as a sphere. Although we were unable to excavate a trench through this ridge to look for an intrusion, we have observed irregular, tabular intrusions of clay in shear zones adjacent to several other ridges exposed in road cuts and stream banks near the Aspen Grove landslide (Fleming and Johnson, 1989).

Deformation Over a Bump in the Failure Surface

A bump in the ground surface that is shaped like half a dome is on the right flank of the Aspen Grove landslide near the 2390-m contour (figs. F1, F26). This bump is referred to henceforth as *the dome*. Several field observations indicated that the dome was growing or deforming. Trees tilted away from the center of the dome (fig. F27), and tension cracks shattered its surface (fig. F27). A quadrilateral (Q–86) and two lines of stakes were set up

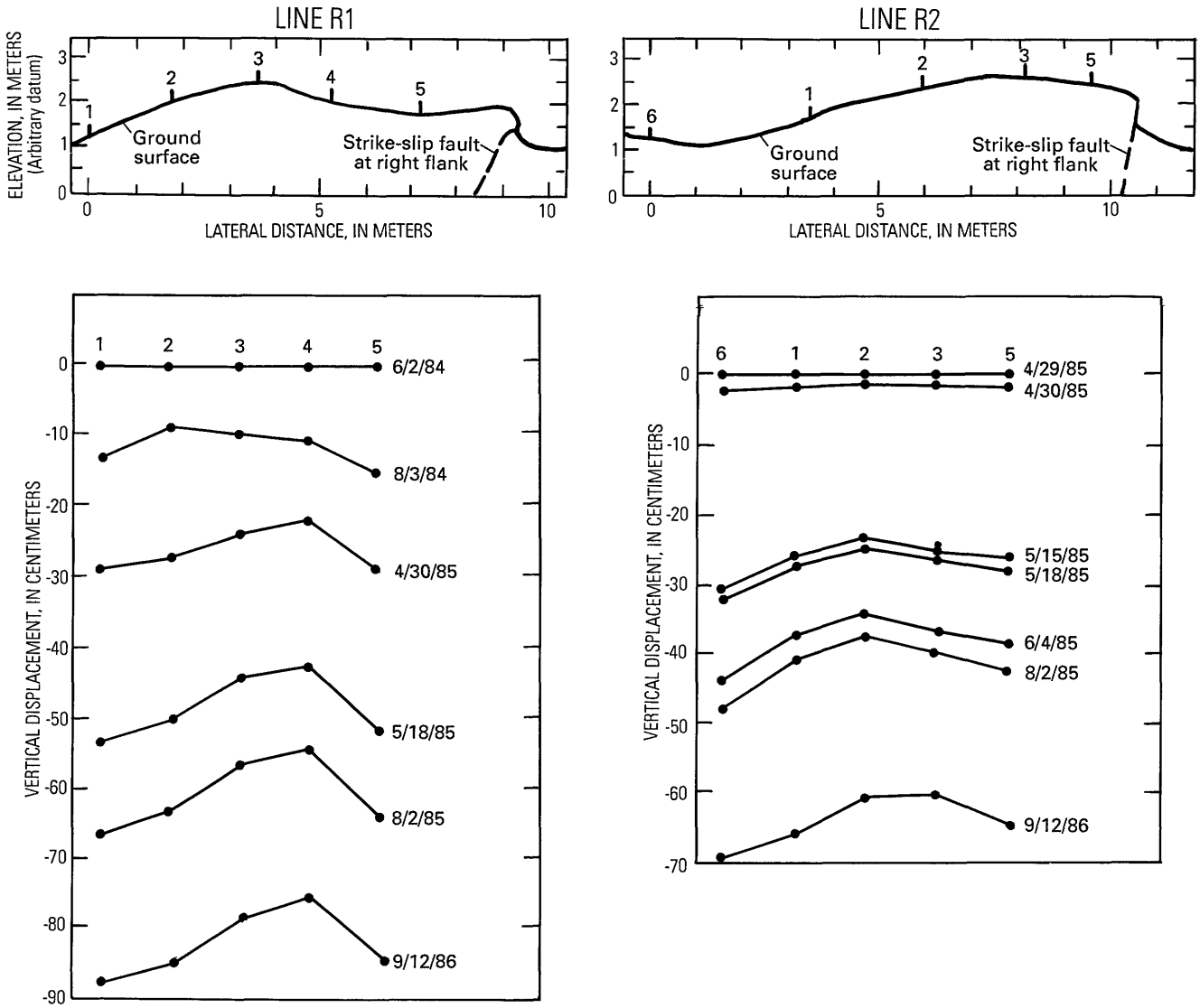

Figure F20 (above and facing page). Profiles and vertical displacement graphs of lines R1, R2, and R3, looking downslope. Stake numbers on the profiles and graphs correspond to those shown in figure F19. Displacement was invariably downward, as indicated by the negative numbers on the displacement graphs. Patterns of vertical displacement on all three lines indicate that the part of the ridge just to the right of center grew in height relative to adjacent parts of the ridge. Although the displacement graph for line R2 shows only data recorded after April 29, 1985, when the last two stakes were added, 1984 data for the three original stakes showed the same pattern: from June 1984 to April 1985, stake 2 was displaced about 5 cm less than stakes 1 and 3.

on the dome (fig. F26) to observe its growth. The dome is one example of a feature at the ground surface that mimics an underlying feature on the slip surface.

The measurements of lines of stakes indicate that the dome is a topographic feature that remains in a fixed location and that the landslide debris passes through it. Figure F28*A* shows the positions of stakes in April and August 1985 along a longitudinal line across the dome—that is, a line parallel to the flank (fig. F26). The longitudinal profile of the dome is well preserved, except for minor thickening at the downslope end of the survey line.

Points crossing the top of the dome rose in absolute elevation during 1985 (fig. F28*B*). Point B3, near the apex of the dome, rose 0.3 m relative to stable ground (DT1). Points on the inside flank of the dome went down about 0.3 m.

A simple two-dimensional model shows how trees that are initially vertical might be tilted as the landslide moves over a bump on the basal slip surface (fig. F29). Trees initially upslope from the bump and on the distal side of the bump (trees 1 and 3, fig. F29) tilt in such a way that they plunge parallel to the direction of displacement. Trees initially on the proximal side of the bump

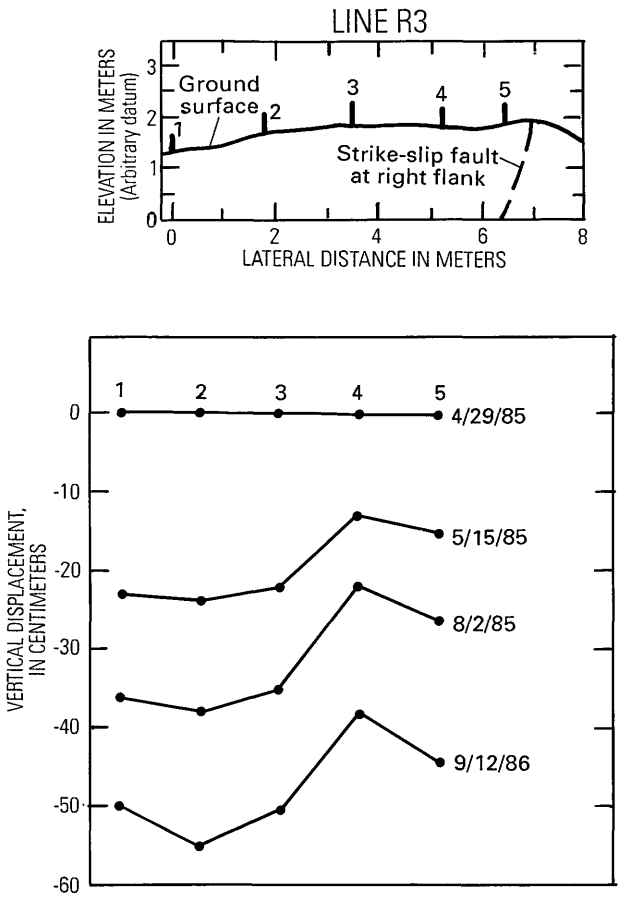

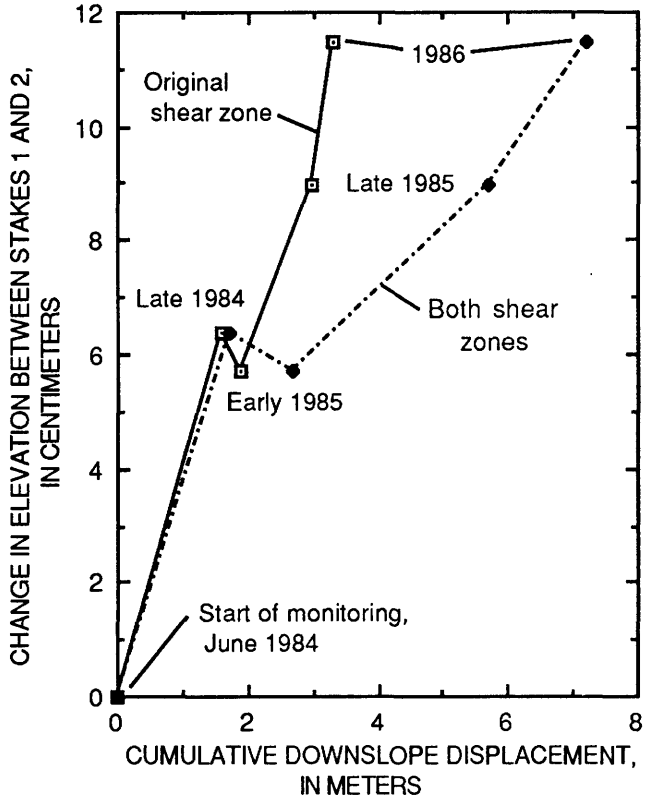

Figure F21. Difference in height between stakes 1 and 2 of line R2 compared to downslope displacement. Squares represent cumulative displacement on the original shear zone (shown as 1983 right flank on fig. F19); triangles represent total displacement on both the original shear zone and the "new" (1984) shear zone (fig. F19). The elevation difference increased almost linearly with displacement except for the anomalous decrease that occurred in early 1985. The ridge grew in height with increasing displacement, even after displacement on the "new" shear zone (5 m west of the ridge) became greater than that on the original shear zone (adjoining the ridge).

(tree 2, fig. F29) tilt in the opposite direction. Trees distal to the bump (tree 4, fig. F29) are, of course, untilted. The pattern of tilting of aspen trees near the right flank (figs. F27 and F30) is similar to the pattern predicted by the model (fig. F29).

Our simple model assumes the landslide deforms by simple shear in a vertical plane, like a deck of cards standing on end, and maintains constant volume and thickness as it traverses the bump. The model accounts neither for longitudinal stretching and shortening nor for thickening and thinning of the material. However, these strains were small compared with the changes due to movement of the debris over the bump in the failure surface. Another model that can also describe the deformation is bending of the material as it slides over the bump. Simple bending would produce deformation qualitatively similar to that produced by simple shear (fig. F29). For simple bending, in which plane surfaces remain planar (Popov, 1968), the ground surface would be approximately parallel with the basal slip surface and the material would thin slightly over the bump. Bending would also produce longitudinal stretching over the crest of the dome, consistent with the formation of cracks in that area (fig. F30*A*).

Other features on the surface of the landslide also appeared to result from deformation over undulations in the basal failure surface. In particular, we observed that the pond near station 150 (pl. F1, figs. F16*B* and *C*) and the pond near station 440 (between the 2350- and 2355-m contours, fig. F1) maintained their positions between 1983 and 1986. The former edges and bottoms of the ponds were observed downslope from the ponds, and trees that had started out upslope from the ponds were later within them.

DISCUSSION AND CONCLUSION

The Aspen Grove landslide generally moved steadily, at a rate that only rarely exceeded 25 cm/d, rather than in surges. The velocity changed gradually, so true steady-state movement was never observed. Sudden movement was measured by extensometers on one occasion. We have not determined whether this was a surge

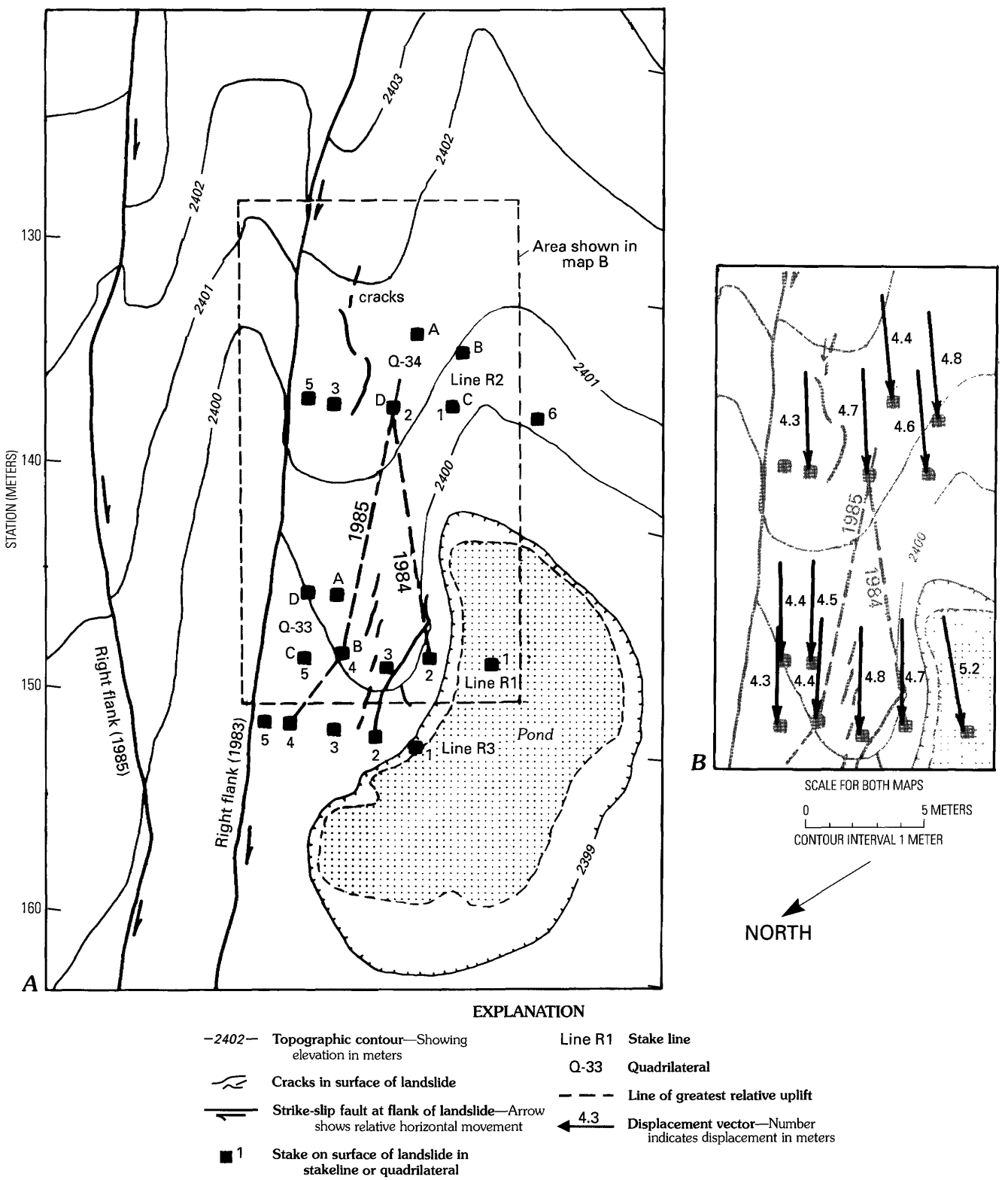

Figure F22. Plane-table maps of the flank ridge near station 150 in August 1985, showing topography, cracks, positions of stakes, and displacement vectors. See figure F1 for location of map area. Heavy dashed lines on both maps connect the stakes having the smallest downward displacement (greatest relative uplift) in 1984 and 1985. Displacement vectors in *B* show horizontal displacement between August 1984 and August 1985. No vectors are shown for stakes 5 and 6 on line R2 because these stakes were not installed until April 1985. Most vectors have a slight component away from the older shear zone (1983 right flank), but some almost parallel the newer shear zone (1985 right flank). The older zone trends N. 51° W. next to the ridge. Stakes that were mapped in August 1984 (fig. F19) and remapped a year later were displaced about 4.5 m along trajectories ranging from N. 56° W. to N. 68° W.

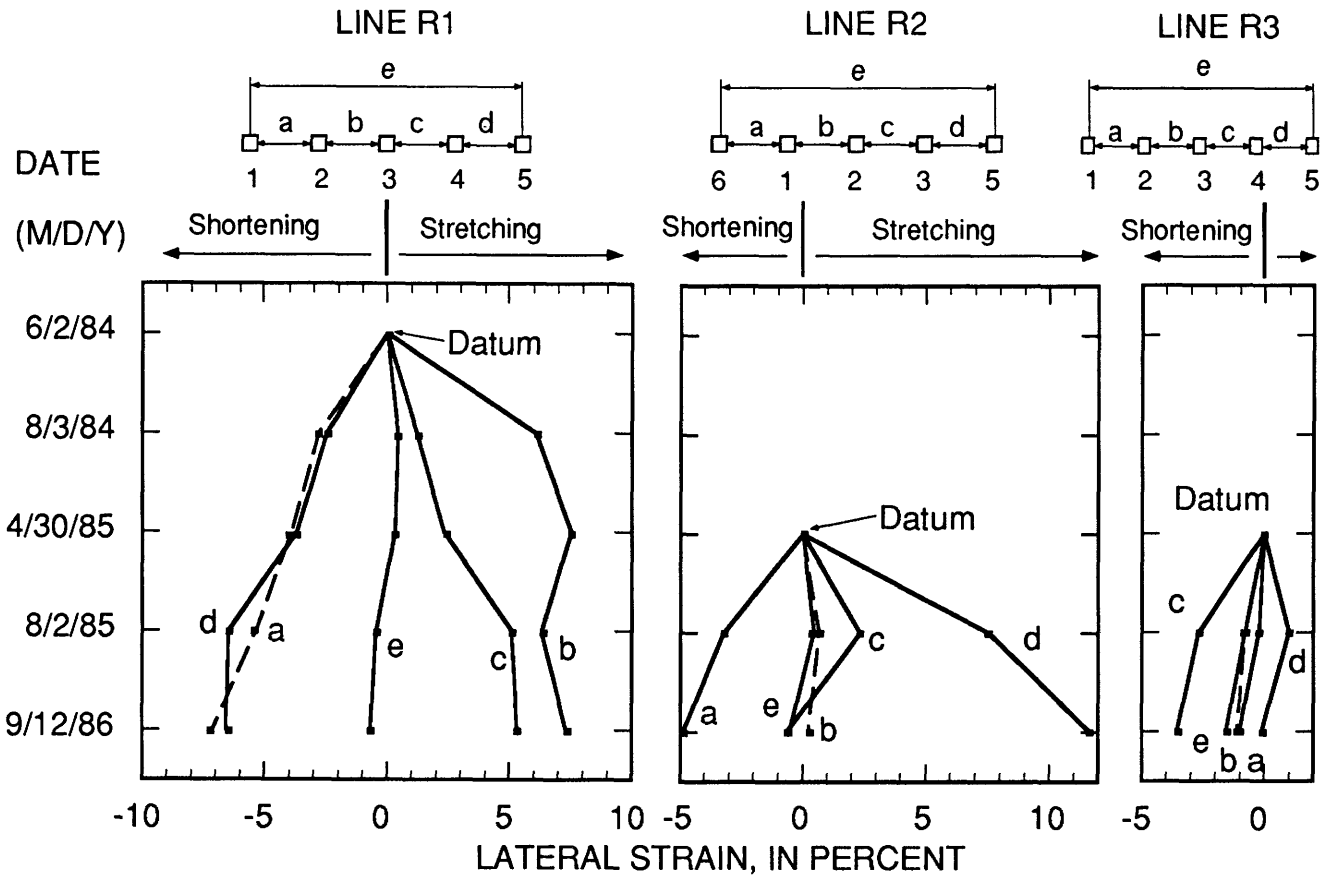

Figure F23. Lateral strain in stake lines R1, R2, and R3 on the flank ridge. Sketches above the graphs show the relative positions of the stakes in plan view; the lower-case letters identify the line segments between consecutive pairs of stakes. The datum in each graph indicates the starting time for computing the cumulative strains in each line of stakes. Overall shortening of the stake lines (*e* on all graphs) was small compared with stretching and shortening in individual segments. Generally, segments near the axis of the ridge (*b* and *c* in line R1 and *c* and *d* in line R2) stretched as segments on the side of the ridge away from the shear zone (segment *a* in each line) shortened. The area of Q–33, which includes segment *d* on line R1, decreased by 2.4–7.4 percent between April and June 1985. The area of Q–34, which incorporates segment *b* of line R2, increased by 2.8 to 7.3 percent between June 1984 and August 1985.

(Hutchinson and others, 1974; Grainger and Kalaugher, 1987), a stick-slip phenomenon (Prior and Stephens, 1972), some other type of movement, or an instrumental error. Overall, the landslide was in mechanical equilibrium during the time it was active. Acceleration of the landslide was negligible compared to gravity during the time that displacement was monitored by recording devices.

Differences in the timing of movement in the main body and the toe of the landslide, shortening between the main body and the toe, and distal enlargement of the landslide from 1983 to 1985 indicate that the main body might drive movement of the toe. In 1986, the toe started moving a day to two weeks later than the main body of the slide and stopped moving a month before the main body. The terminus of the landslide gradually propagated downslope as the landslide material shortened longitudinally; the apparent terminus was about 600 m downslope from the head in 1983, and toes, partially defining the

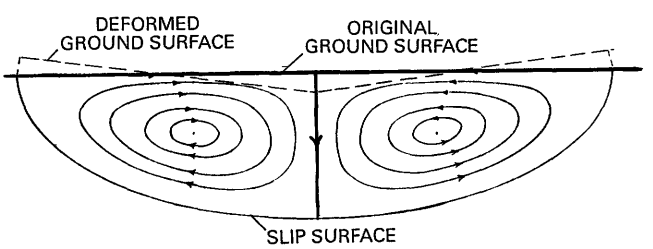

Figure F24. Helical flow pattern indicated by displacement of points on the surface of the flank ridge (modified from diagram by Rivlin, 1964, showing secondary flow pattern in an elliptic pipe). The helical flow pattern indicates that points near the flanks should be gradually transported upward to the surface and then toward the center as the material flows downslope. Thus, points at the surface should follow trajectories that make an acute angle with the side of the channel.

Table F3. Displacement of stakes in quadrilateral Q–2 on the flank ridge near station 120

Period of observation	Stake Q–2A		Stake Q–2B	
	Divergence from flank[1]	Displacement (cm)	Divergence from flank[1]	Displacement (cm)
6/15/83–8/4/83	10.2°	14	11.4°	16
8/4/83 –5/23/84	5.4°	222	7.2°	216
5/23/84–8/3/84	13.0°	159	11.8°	160
8/3/84 –4/28/85	24.5°	29	31.2°	30
4/28/85–8/2/85	9.6°	108	8.0°	106
8/2/85 –9/12/86	15.4°	32	4.6°	33
Cumulative:				
6/15/83–9/12/86	10.2°	564		

[1]Angle measured in the horizontal, counterclockwise from the vertical plane containing the 1983 shear zone (right flank) to the vertical plane containing the displacement vector.

terminus, finally formed about 1,000 m downslope from the head in 1985.

Much deformation observed in the landslide can be attributed to the geometry of the landslide boundaries. The landslide stretched axially where it slid between converging flanks (except between stations 380 and 450, where it shortened), and shortened axially between diverging flanks (pl. F1, fig. F12). Conversely, it apparently shortened transversely between converging flanks and stretched transversely between diverging flanks; little material spilled over the flanks where they converge and shear zones did not dilate appreciably where the flanks diverge. Features at the surface of the landslide, such as the ponds at stations 150 and 440 and the dome near station 250, mimic irregularities on the basal slip surface. The velocity varies laterally where the landslide is forced to bend at turns in the flanks, or to squeeze between converging flanks (fig. F13). These observations lead us to suggest that uneven boundaries might retard landslide movement by causing landslide debris to deform. Mizuno (1989) and

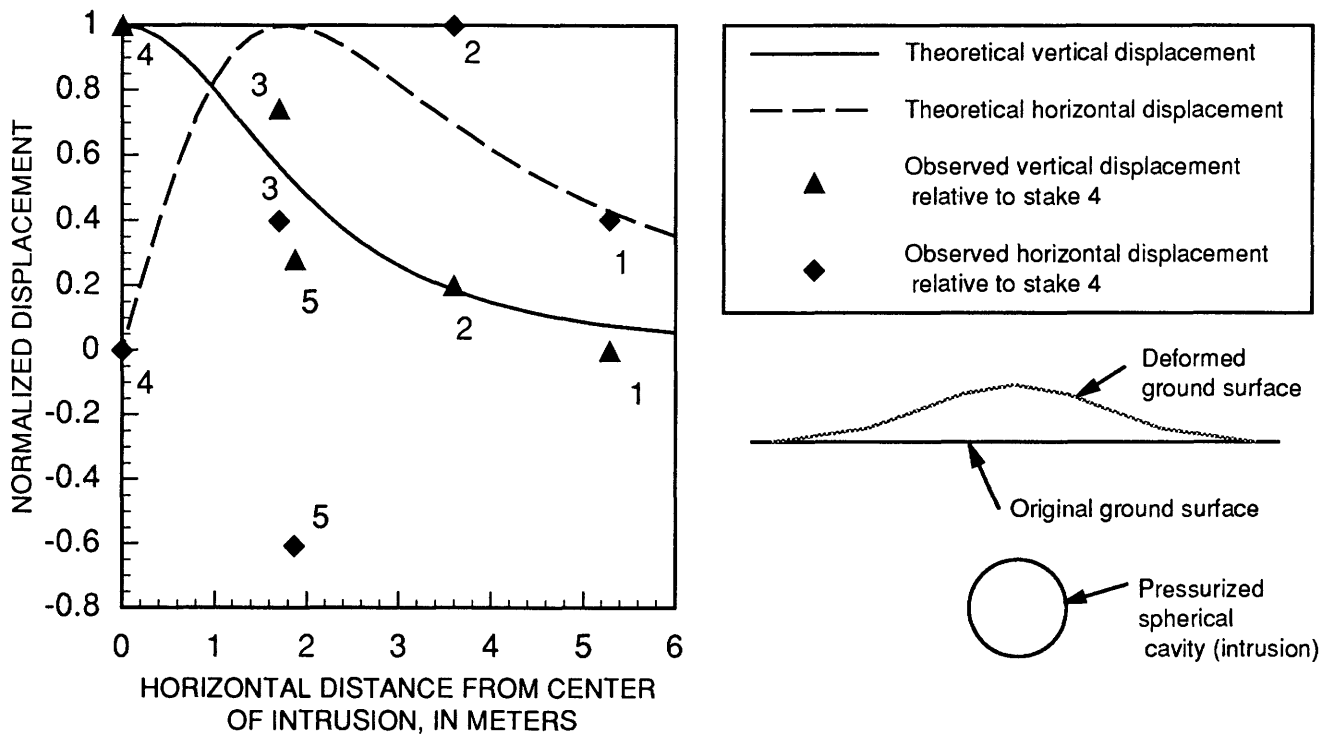

Figure F25. Deformation at the ground surface above a theoretical intrusion compared with deformation at line R1 on the ridge. The intrusion is modeled as a pressurized, spherical cavity 10 cm in diameter and 2.5 m deep in an elastic half-space (Mogi, 1958, p. 104–105). Displacements are plotted as relative proportions of their maximum values. Vertical displacements are positive upward; stakes 2–5 moved upward relative to stake 1. Horizontal displacements are positive if directed away from the intrusion. The center of the intrusion is probably somewhere between stakes 3 and 4, but stake 4 is assumed to be over the center for convenience in plotting and computing horizontal displacements. The observed displacements are for the period from June 2, 1984, to September 12, 1986. Stake numbers are indicated beside data points. Relative vertical displacement was greatest at stake 4, and decreased with increasing distance from stake 4, consistent with theory. Relative horizontal displacement appears consistent with predicted lateral stretching near the intrusion and lateral shortening away from the intrusion, despite anomalous shortening between stakes 4 and 5.

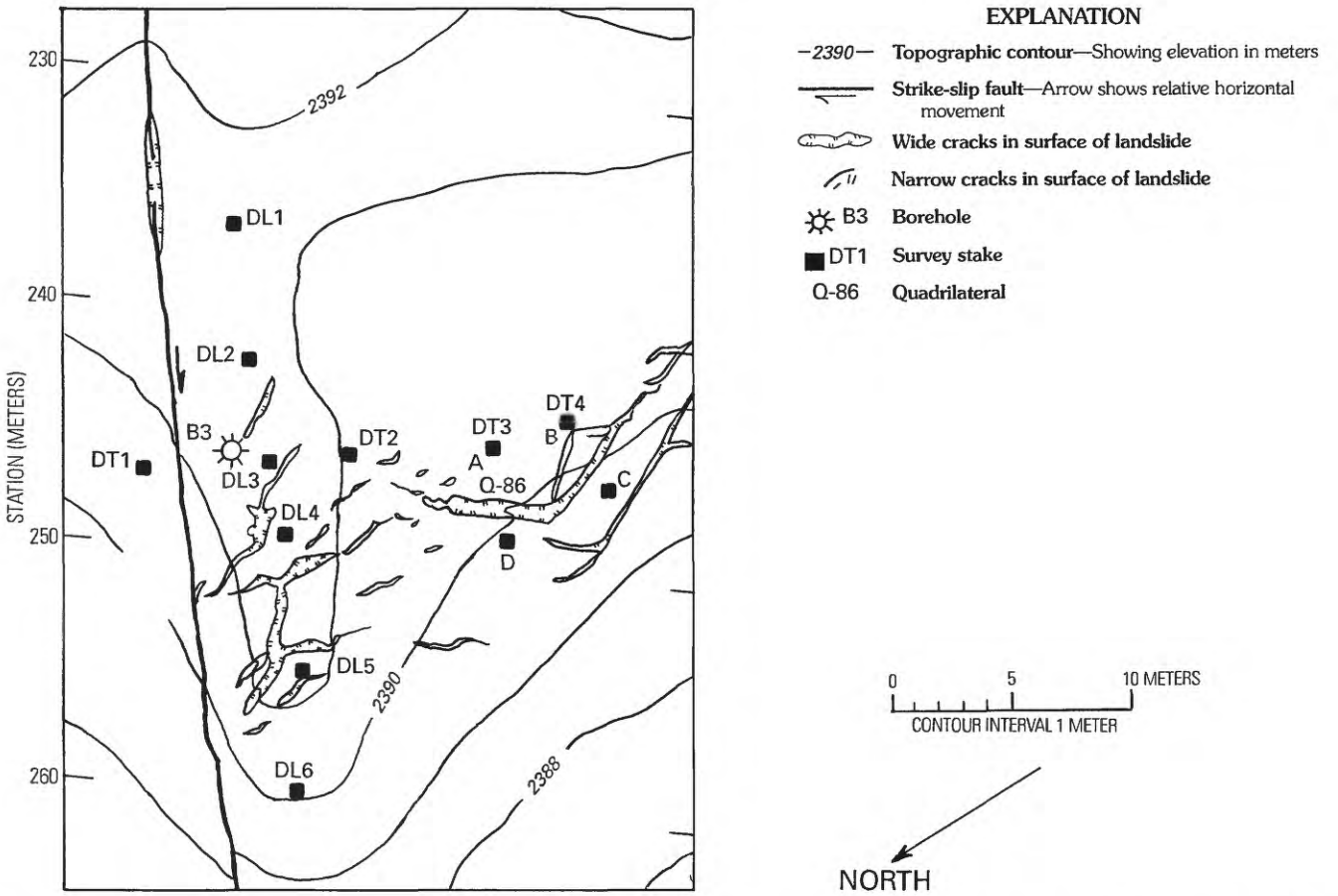

Figure F26. Plane-table map of the dome near station 250 at the beginning of movement in 1985, showing topography, cracks, and positions of stakes. The dome, actually a half-dome, was a conspicuous topographic feature on the flank of the landslide in 1984 and superficially resembled a flank ridge. The dome is about 30 m long, 15 m wide, and 1.5 m high. Tension cracks appeared in the crest of the dome in the spring of 1984 and enlarged throughout the summer. Topography and cracks were mapped in August 1984. Stakes were installed in April 1985.

Baum and Johnson (1993) analyzed two possible models for movement of landslides having uneven boundaries.

Most of the displacement occurring near the axis of the landslide results from shear at the boundaries (sliding on slip surfaces). Measurements indicated that from 82 to 97 percent of the movement results from boundary shear. The remainder results from internal shear of the landslide material; Crandell and Varnes (1961), Hutchinson (1970), Harden and others (1978), and Keefer and Johnson (1983) report similar results for several other landslides.

We monitored the deformation of a flank ridge in detail in order to understand how it formed. The orientation of displacement vectors is consistent with a type of circulation or secondary deformation (fig. F24) that occurs in materials having nonlinear rheologies (Rivlin, 1964; Truesdell, 1964; McTigue and others, 1985), but its growth in height seems more consistent with the intrusion of material from beneath the ridge (fig. F25), somewhat like intrusion of magma beneath a volcano before an eruption (Mogi, 1958; Eaton, 1959; Richter and others, 1964; Fiske and Koyanagi, 1968). We have seen evidence of intrusion of clay at the flanks of several other landslides in central Utah (Fleming and Johnson, 1989). We have also seen flank ridges on some other landslides that have features more consistent with the helical flow models (fig. F24). Our observations leave several questions about ridges unanswered: Why are ridges active during some episodes of movement but not during others? Why do ridges occur only locally, rather than all along the flanks of landslides? Why are ridges not all in the same geometric setting? They occur in converging, diverging, straight, and curved parts of landslides.

REFERENCES CITED

Baum, R.L., 1988, The Aspen Grove landslide, Ephraim Canyon, central Utah: Cincinnati, Ohio, University of Cincinnati, Ph.D. thesis, 363 p.

Baum, R.L., and Fleming, R.W., 1989, Landslides and debris flows in Ephraim Canyon, central Utah, chap. C *of* Landslide

Figure F27. Leaning trees on the dome in July 1985. View to the north. Trees upslope (right in photograph) from the dome lean to the right; those downslope lean to the left. Trees in foreground (on the side of the dome) lean toward the observer. Displacement direction is from right to left.

processes in Utah—Observation and theory: U.S. Geological Survey Bulletin 1842, p. C1–C12, 1 oversize plate.

_____1991, Use of longitudinal strain in identifying driving and resisting elements of landslides: Geological Society of America Bulletin, v. 103, p. 1121–1132.

Baum, R.L., Fleming, R.W., and Ellen, S.D., 1989, Maps showing landslide features and related ground deformation in the Woodlawn area of the Manoa valley, City and County of Honolulu, Hawaii: U.S. Geological Survey Open-File Report 89–290, 16 p., 2 plates.

Baum, R.L., and Johnson, A.M., 1993, Steady movement of landslides in fine-grained soils—A model for sliding over an irregular slip surface, chap. D *of* Landslide processes in Utah—Observation and theory: U.S. Geological Survey Bulletin 1842, p. D1–D28.

Baum, R.L., Johnson, A.M., and Fleming, R.W., 1988, Measurement of slope deformation using quadrilaterals, chap. B *of* Landslide processes in Utah—Observation and theory: U.S. Geological Survey Bulletin 1842, p. B1–B23.

Crandell, D.R., and Varnes, D.J., 1961, Movement of the Slumgullion earthflow near Lake City, Colorado, art. 57 *in* Short papers in the geologic and hydrologic sciences: U.S. Geological Survey Professional Paper 424–B, p. B136–B139.

Crozier, M.J., 1984, Field assessment of slope instability, *in* Brunsden, Denys, and Prior, D.B., eds., Slope instability: New York, Wiley, p. 103–140.

Eaton, J.P., 1959, A portable water-tube tiltmeter: Bulletin of the Seismological Society of America, v. 49, no. 4, p. 301–316.

Fiske, R.S., and Koyanagi, R.Y., 1968, The December 1965 eruption of Kilauea Volcano, Hawaii: U.S. Geological Survey Professional Paper 607, 21 p.

Fleming, R.W., and Johnson, A.M., 1989, Structures associated with strike-slip faults that bound landslide elements, *in* Johnson, A.M., Burnham, C.W., Allen, C.A., and Muehlberger, W., eds., Richard H. Jahns Memorial Volume: Engineering Geology, v. 27, nos. 1–4, p. 39–114.

Grainger, P., and Kalaugher, P.G., 1987, Intermittent surging movements of a coastal landslide: Earth Surface Processes and Landforms, v. 12, p. 597–603.

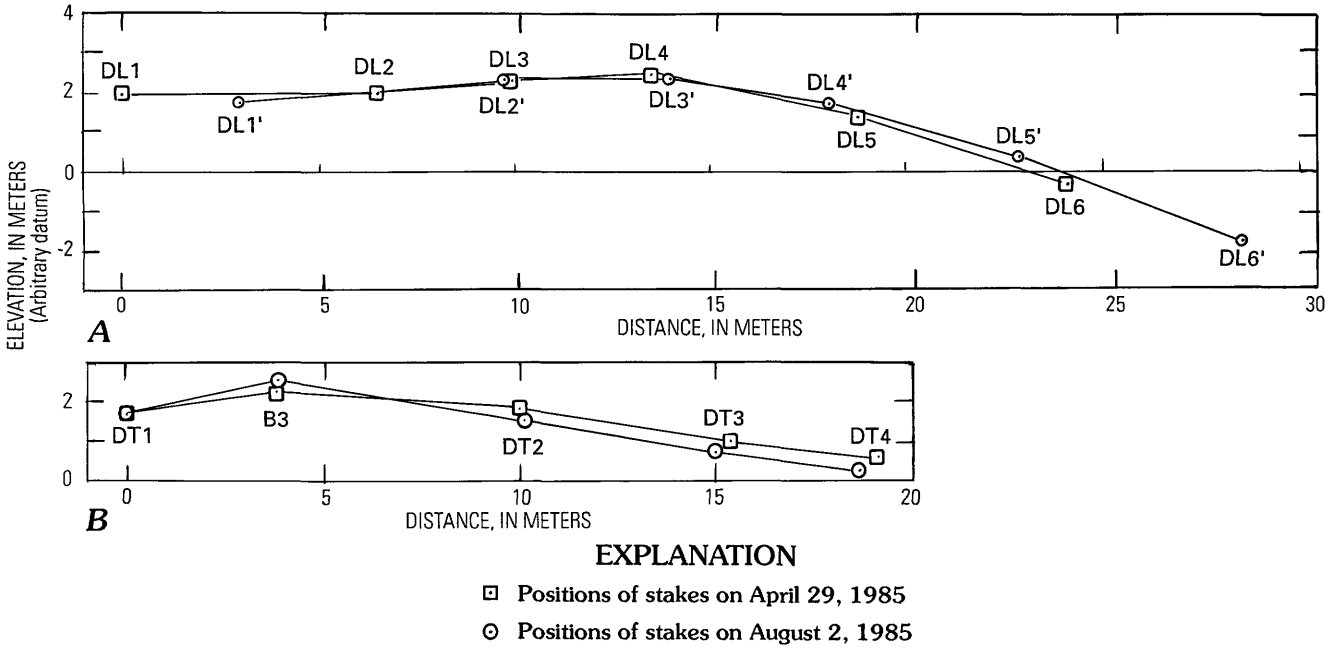

Figure F28. Profiles of stake lines across the dome near station 250 showing displacement between April 29 and August 2, 1985. See figure F26 for location of stake lines. Elevations of stakes were referenced to a stable point off the landslide. *A*, Vertical and longitudinal displacement along line DL. The average downslope movement near the dome during the time represented was about 3 m, so the August horizontal position of the first stake (DL1) is displaced 3 m to the right of its April position. Positions of other stakes are relative to DL1. The longitudinal profile of the dome is preserved as landslide debris is transported over it. *B*, Vertical and lateral displacement along line DT. Lateral displacement is relative to stake DT1, which was off the landslide and maintained a constant vertical and lateral position. In terms of absolute elevation, stakes DT2, DT3, and DT4 descended, but point B3, at the crest of the dome, rose.

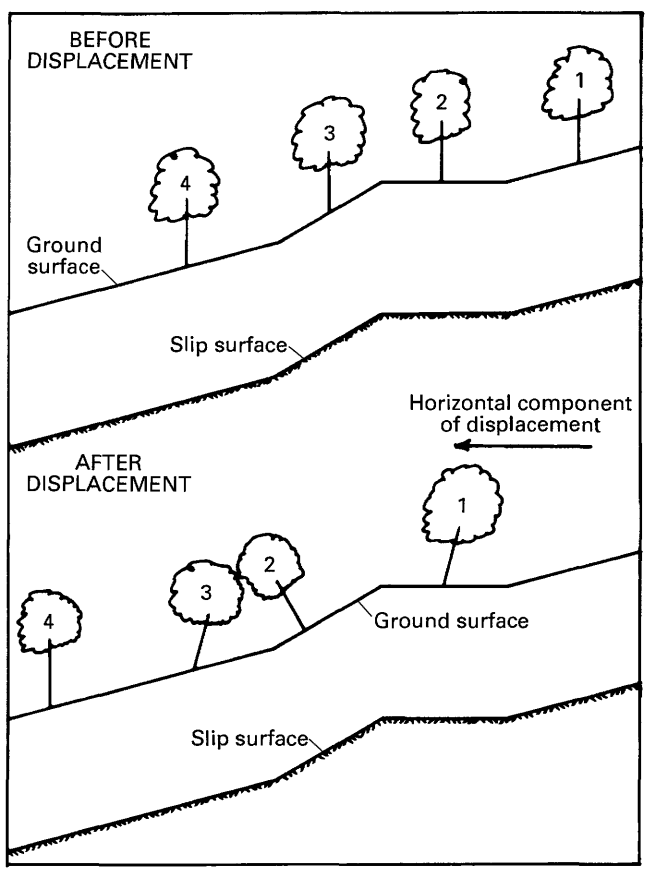

Figure F29. Diagram showing how trees that were initially vertical are tilted as the landslide moves over a bump on the slip surface. The diagram was constructed by assuming that vertical planes in the landslide debris remain vertical during displacement. Trees 1 and 3 move to flatter ground and tilt towards the right (so that in map view they plunge parallel to the direction of displacement), tree 2 moves to steeper ground and tilts to the left, plunging antiparallel to the direction of displacement, and tree 4 moves on a constant slope and remains vertical.

Hadley, J.B., 1964, Landslides and related phenomena accompanying the Hebgen Lake earthquake of August 17, 1959, *in* The Hebgen Lake earthquake of August 17, 1959: U.S. Geological Survey Professional Paper 435, p. 107–138.

Harden, D.R., Janda, R.J., and Nolan, K.M., 1978, Mass movements and storms in the drainage basin of Redwood Creek, Humboldt County, California—A progress report: U.S. Geological Survey Open-File Report 78–486, 161 p.

Hill, R., 1950, The mathematical theory of plasticity: London, Oxford University Press, 356 p.

Hutchinson, J.N., 1970, A coastal mudflow on the London clay cliffs at Beltinge, north Kent [England]: Géotechnique, v. 20, no. 3, p. 235–252.

Hutchinson, J.N., Prior, D.B., and Stephens, Nicholas, 1974, Potentially dangerous surges in an Antrim [Ireland] mudslide: Quarterly Journal of Engineering Geology, v. 7, no. 4, p. 363–376.

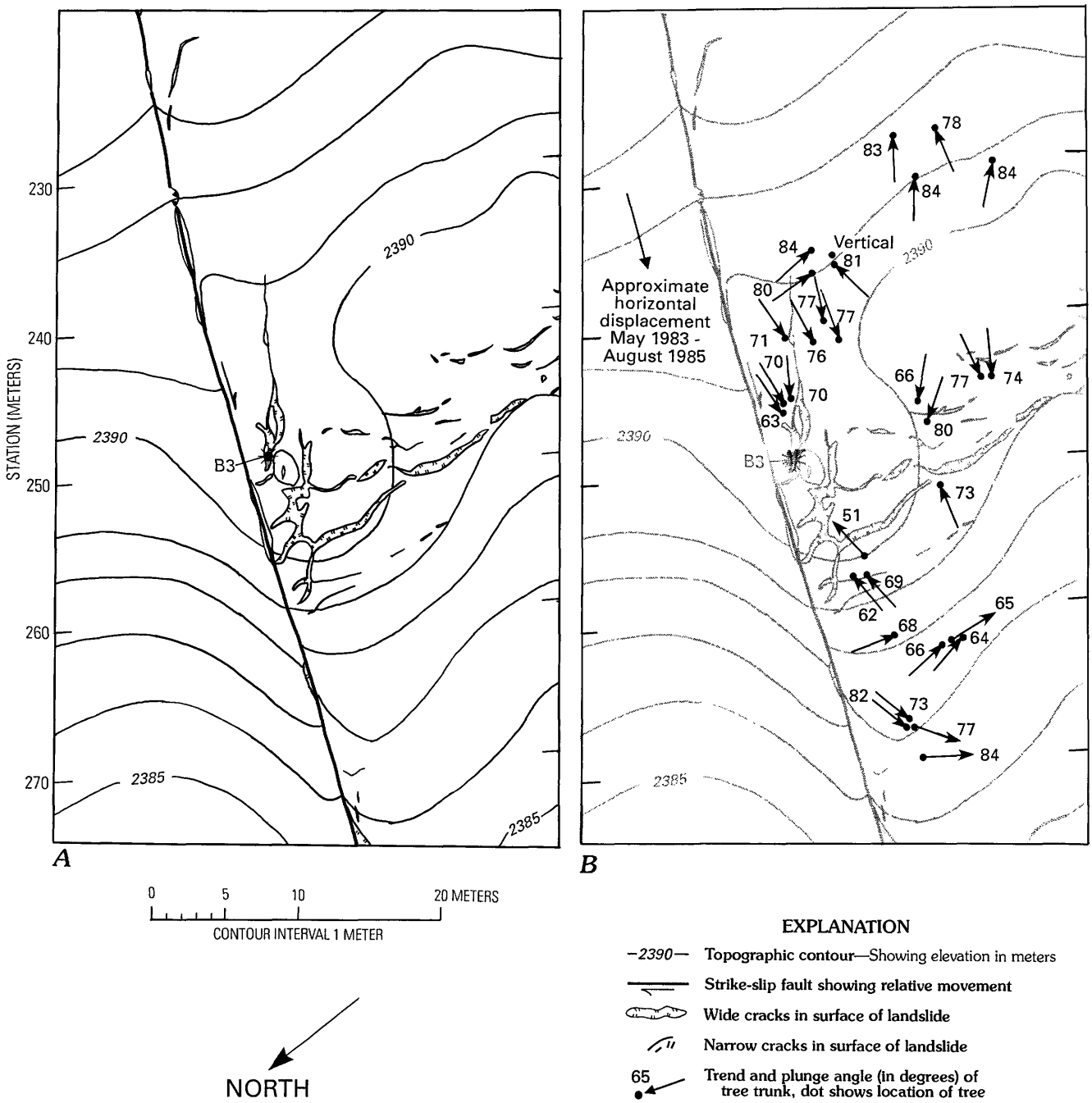

Figure F30. Plane-table maps of the dome near station 250 as of August 2, 1985, showing cracks in the landslide surface (A) and trends and plunge angles of inclined trees near the dome (B). In B, trees proximal to the crest of the dome (between the 2390- and 2391-m contours) plunge 63°–77° toward the west, roughly parallel to the direction of displacement. Trees distal to the crest of the dome (between the 2389- and 2390-m contours) plunge 51°–73° toward the east, roughly antiparallel to the direction of displacement. Trees opposite borehole B3, distal to the dome, plunge 73°–84° toward the west or southwest, roughly parallel to the direction of displacement. Tilt is consistent with displacement of landslide debris of constant thickness over a bump in the failure surface.

Iverson, R.M., 1986, Unsteady, nonuniform landslide motion—2. Linearized theory and the kinematics of transient response: Journal of Geology, v. 94, p. 349–364.

Johnson, A.M., and Baum, R.L., 1987, BASIC programs for computing displacements, strains, and tilts from quadrilateral measurements: U.S. Geological Survey Open-File Report 87–343, 19 p.

Keefer, D.K., and Johnson, A.M., 1983, Earth flows—Morphology, mobilization, and movement: U.S. Geological Survey Professional Paper 1264, 56 p.

Lantz, J.R., 1984, Geology and kinematics of a clay-rich landslide with an undulatory slip surface: College Station, Tex., Texas A&M University, M.S. thesis, 132 p.

Malvern, L.E., 1969, Introduction to the mechanics of a continuous medium: Englewood Cliffs, N.J., Prentice-Hall, 713 p.

McTigue, D.F., Passman, S.L., and Jones, S.F., 1985, Normal stress effects in the creep of ice: Journal of Glaciology, v. 31, no. 108, p. 120–126.

Mizuno, K., 1989, Landsliding of clayey slopes with wavy slip surface—Model and its application: Japan, Science Reports of the Institute of Geoscience, Tsukuba, sec. A, v. 10, p. 87–151.

Mogi, Kiyoo, 1958, Relations between the eruptions of various volcanoes and the deformations of the ground surfaces around them: Bulletin of the Earthquake Research Institute, v. 36, p. 99–134.

Nye, J.F., 1965, The flow of a glacier in a channel of rectangular, elliptic, or parabolic cross section: Journal of Glaciology, v. 5, no. 41, p. 661–690.

Oberste-Lehn, Deane, 1976, Slope stability of the Lomerias Muertas area, San Benito County, California: Stanford, California, Stanford University, Ph.D. thesis, 216 p.

Popov, E.P., 1968, Introduction to mechanics of solids: Englewood Cliffs. N.J., Prentice-Hall, 571 p.

Prior, D.B., and Stephens, N., 1972, Some movement patterns of temperate mudflows—Examples from northeastern Ireland: Geological Society of America Bulletin, v. 83, no. 8, p. 2533–2543.

Richter, D.H., Ault, W.U., Eaton, J.P., and Moore, J.G., 1964, The 1961 eruption of the Kilauea Volcano, Hawaii: U.S. Geological Survey Professional Paper 474–D, p. D1–D34.

Rivlin, R.S., 1964, Second and higher order theories for the flow of a viscoelastic fluid in a noncircular pipe, *in* Proceedings of the International Symposium on Second Order Effects, International Union of Theoretical and Applied Mechanics, Haifa, Israel, 1962: New York, Macmillan Co., p. 668–677.

Rybář, Jan, 1968, Ein Beispiel von Bewegungsmessungen an Rutschungen: Zeitschrift fr Angewandte Geologie, v. 14, no. 3, p. 138–141.

Skopek, J., Rybář, J., and Dobr, J., 1972, Pore-water pressure observations in a landslide: Proceedings of the 24th International Geological Congress, Montreal, Canada, sec. 13, p. 150–159.

Ter-Stepanian, George, 1965, *In-situ* determination of the rheological characteristics of soil on slopes, *in* Proceedings of the Sixth International Conference on Soil Mechanics and Foundation Engineering: Montreal, Canada, University of Toronto Press, v. 2, p. 575–577.

_____1984, Analysis of slope deformation for determining the landslide mechanism, *in* Proceedings of the Fourth International Symposium on Landslides, v. 2: Downview, Ontario, Canada, University of Toronto Press, p. 499–504.

Truesdell, C., 1964, Second-order effects in the mechanics of materials, *in* Proceedings of the International Symposium on Second Order Effects, International Union of Theoretical and Applied Mechanics, Haifa, Israel, 1962: New York, Macmillan Co., p. 1–47.

Van Asch, Th.J.W., and Van Genuchten, P.M.B., 1990, A comparison between theoretical and measured creep profiles of landslides: Geomorphology, v. 3, p. 45–55.

Varnes, D.J., 1978, Slope movement types and processes, chap. 2 *of* Schuster, R.L., and Krizek, R.S., eds., Landslides—Analysis and control: U.S. National Academy of Sciences, Transportation Research Board Special Report 176, p. 11–33.

Zaruba, Quido, and Mencl, Vojtech, 1982, Landslides and their control, 2d revised edition: New York, Elsevier, 324 p.

Manuscript approved for publication April 1, 1993.
Published in the Central Region, Denver, Colorado.
Photocomposition by Debra Sokol.
Graphics by Gayle M. Dumonceaux.
Edited by Peter L. Martin.

APPENDIX—METHODS AND ACCURACY OF MEASUREMENTS

Wooden stakes were used at the corners of quadrilaterals and in stake lines. A small finishing nail was driven into the top of each stake to serve as a measuring point. Positions of stakes in transverse stake lines were measured by holding a string taut between the reference stakes, which were beyond the edges of the landslide, holding a tape perpendicular to the string and measuring to a plumb line positioned over each stake. Sometimes we located the stakes by making a plane-table map of the stakes on the landslide and the reference stakes. Longitudinal stake lines and quadrilaterals were measured by hooking a steel tape on one nail and measuring the distance to adjacent stakes. Elevations of the tops of the stakes were measured by taking backsights with a precision level. Details of the use of quadrilaterals are described in Baum and others (1988).

The precision of the measurements varied with the techniques and instruments used. Measurements between adjacent stakes made with a steel tape usually could be repeated to within 3 mm; however, errors of 6 mm were sometimes observed and larger errors might exist in some of the measurements. Our average precision in measuring the downslope displacements of stakes in the transverse lines was probably about 5 to 8 cm. Elevations measured with the precision level were repeatable to about 0.5 mm. Displacements of most points amounted to tens or hundreds of centimeters each year; therefore, the precision of our measurements was adequate to determine the displacements.

True accuracy of the stake measurements is difficult to assess. In addition to the difficulty of reproducing a specific measurement under ideal conditions, problems such as tilting of stakes between measurements, mistakes in reading or recording measurements, and difficulties in making the actual measurements in the field further decreased the accuracy of our measurements. Where we had many sets of measurements, as for the quadrilaterals, we eliminated many inaccurate measurements by discarding those that departed significantly from a steady trend or constant value (before and after) through time. From the remaining quadrilateral measurements, we used those having the smallest errors of closure to compute strains and felt confident that we could resolve strains as small as ±0.003 (±0.3 percent) and displacements as small as 1 cm (Baum and others, 1988). Similarly, we feel confident that measurements of distances between neighboring stakes in a line, such as lines R1, R2, and R3 on the flank ridge, can resolve changes as small as ±1 cm. Because measurement of longitudinal displacement was difficult on long transverse lines of stakes, such as lines U, M, and L, we could only resolve displacements greater than about 10 cm on these lines.

The recording extensometers were water-level recorders (slightly modified) of the type used by U.S. Geological Survey hydrologists. Each recorder was placed in a wooden box attached to a tree just outside the flank of the landslide. One end of a fine stainless steel wire was hooked to another tree just inside the flank of the landslide, a few meters downslope from the recorder. The other end of the wire was attached to and wrapped around the recorder flywheel. A counterweight, hung from a second wire that was wrapped in the opposite direction around a small hub on the recorder flywheel, kept tension in the stainless steel wire. As the landslide moved, the stainless steel wire uncoiled and caused the flywheel to rotate. A clock activated the recorder every fifteen minutes, causing it to punch a tape. Later, in the office, the data were read from the tape and plotted as time-displacement curves.

Several factors can affect the accuracy of measurements made by recording extensometers: (1) Diurnal temperature variations can cause the wire to change length by 1 to 2 mm over the course of a day. (2) Sagging of the wire can introduce cumulative errors of a few centimeters over the course of a few meters displacement. (3) Misalignment of 5° between the wire and the direction of displacement causes cumulative errors of a few centimeters in measuring a total displacement of 10 m. We could confidently resolve displacement of approximately 2 mm in a period of 24 hours. It is difficult to make corrections for any of these without making additional measurements. However, the accuracy of the extensometer data was judged adequate because other methods of measuring displacements were subject to errors as large as those in the extensometer data or larger.

☆U.S. GOVERNMENT PRINTING OFFICE: 1993-573-038/86007